2022

1-D Crustal Seismic Velocity Models for West-Central and Western Montana

Courtenay Duzet
University of Montana, Missoula

1-D SEISMIC VELOCITY MODELS FOR WEST-CENTRAL AND WESTERN MONTANA

By

COURTENAY JO DUZET

Bachelor of Science in Environmental Sciences & Earth Systems, Oregon State University, Corvallis, Oregon, 2018

Thesis

presented in partial fulfillment of the requirements
for the degree of

Master of Science
in Geosciences

The University of Montana
Missoula, MT

May 2022

Approved by:

Scott Whittenburg,
Graduate School Dean

Dr. Hilary Martens, Chair
Geosciences

Dr. Joel Harper
Geosciences

Dr. Paul Janzen
Physics

Dr. Michael Stickney
Montana Bureau of Mines and Geology

Duzet, Courtenay, M.S, May 2022 *Geosciences*

1-D Seismic Velocity Models for West-Central and Western Montana

Chairperson: Dr. Hilary Martens

In seismically active areas with infrequent, large-magnitude earthquakes, high-quality seismic data are critical for determining high-resolution, accurate seismic velocity models. Here, we present a new local-scale seismic velocity model for the crust in west-central Montana as well as a new regional-scale seismic velocity model for the crust and upper mantle across broader western Montana. The new models are constrained by phase arrivals from several passive seismic networks, including the University of Montana Seismic Network (UMSN), the Montana Regional Seismic Network (MRSN), the Advanced National Seismic System (ANSS), temporary deployments by the United States Geological Survey (USGS), and the USArray Transportable Array (TA). We invert jointly for hypocenters and velocity structure using the VELEST software. The "local" seismic velocity model is the first model specific to west-central Montana, constrained primarily by P-wave arrivals from aftershocks that followed the 2017 M 5.8 Lincoln, Montana, earthquake. The Lincoln earthquake is the largest event to occur in western Montana in more than half a century. The local model consists of eight distinct layers down to 30 km depth below mean sea level and spans a region of about 40,000 km^2 (200 km by 200 km). The velocity of the upper-most layer in the local model is 4.80 ± 0.12 km/s and the velocity of the lower-most layer is 7.00 ± 0.05 km/s. Additionally, we estimate station corrections for 50 stations that have operated in Montana during the period 2017-2021. Using an expanded dataset across a broader geographical area, we develop a "regional" seismic velocity model that represents spatially averaged velocity structure across western Montana. A larger geographical scope and deeper ray paths allow the estimation of the velocity structure of the deep crust and upper mantle. The regional model consists of thirteen distinct layers down to 45 km depth below sea level and is appropriate to an area of about 160,000 km^2 (400 km by 400 km). The velocity of the upper-most layer is 4.30 ± 0.07 km/s and the velocity of the lower-most layer is 8.00 ± 0.04 km/s. The new models are similar to prior velocity models for western Montana and include enhanced depth resolution. We find that the new local model for west-central Montana revises the hypocenter locations of Lincoln aftershocks by about 0.89 km on average.

Table of Contents

1. Background and Motivation

Seismic velocity models are essential for determining earthquake hypocenters and focal mechanisms. Empirically constrained seismic velocity models also shed light on crustal lithology (Matrullo *et al*., 2013). While Montana experiences thousands of earthquakes every year, most events are small in magnitude (<M2; Stickney *et al.,* 2000). These low-magnitude earthquakes do not typically produce enough seismic energy to be well recorded on regional seismic networks with enough data to develop well-constrained seismic velocity models, except on local scales. Large-magnitude events (> M5), followed by vigorous aftershock sequences, generate numerous earthquakes useful for constraining the seismic velocity structure; however, M5+ events have been infrequent in Montana since instrumental monitoring improved in the 1980s with the inception of the Montana Regional Seismic Network (MRSN; Stickney 2022). Only four M5+ events have occurred in Montana since 1980 (Stickney 2022).

1.1 Geological Context

Earthquakes in western Montana occur within a zone of concentrated intraplate deformation (Stickney, 2015; Smith *et al.,* 2021). The Intermountain Seismic Belt (ISB), a north-south trending fault of seismicity that transects the Intermountain West, extends through western Montana and into southern Nevada and northwestern Arizona (Smith and Arabasz, 1991). Another distinct zone of seismic activity, known as the Centennial Tectonic Belt (CTB), branches westward into central Idaho from southwest Montana (Stickney and Bartholomew, 1987, Mason, 1996). The ISB and CTB are characterized by predominantly shallow (less than 20 km in depth) seismicity influenced by preexisting geologic structures and tectonic interactions between the Snake River Plain, the Yellowstone volcanic system, the Northern Rocky Mountains, and the Great Plains

provinces (Stickney, 2015; Doser, 1989). Western Montana is also transected by a fault zone known as the Lewis and Clark Line (LCL), a complex shear zone that extends from northern Idaho to Helena, Montana. The LCL consists of at least a dozen major faults with slip histories going back to at least the Laramide Orogeny, which influence regional deformation (Wallace et al., 1990; Sears and Hendrix, 2004; Stickney, 2015).

1.2 Previous Seismic Velocity Models for Western Montana

The seismic velocity model commonly adopted for western Montana in the past two decades was derived using the first-arriving P-wave travel times of 1432 well-recorded earthquakes in southwest Montana (Zeiler et al., 2005). Using an iterative inversion process, they estimated P-wave velocities in the crust ranging from 5.70 km/s to 6.53 km/s, with an upper-mantle velocity of 8.0 km/s below an estimated Moho depth of 39.7 km.

Two other seismic velocity models were previously derived in 1984 (Sheriff and Stickney, 1984) and 1997 (Stickney, 1997). The 1984 model was derived using an east-central Idaho seismic velocity model as a reference and a reversed refraction profile that utilized open pit mine blasts in Butte, MT and Challis, ID (Sheriff & Stickney, 1984). The 1984 model estimated crustal velocities between 4.80 km/s and 6.80 km/s, an upper-mantle velocity of 8.0 km/s below a depth of 40 km, and crustal-thickness uncertainties up to 8 km due to the limited resolution of the lower crustal layers (Sheriff & Stickney, 1984; Stickney, 1984).

The 1997 seismic velocity model was constrained by first-arriving P-waves from 1200 earthquakes and 14 mining blasts from the southwest region of Montana (Stickney, 1997). Stickney (1997) simultaneously inverted for seismic velocities and layer

thicknesses to develop the 1-D model. The 1997 model reported crustal velocities of 5.52 km/s to 6.74 km/s with an upper mantle velocity of 8.0 km/s below a depth of 38.7 km.

Lacking large-magnitude earthquakes and with limited seismic network coverage at the time (Stickney, 2022), the 1984, 1997, and 2005 models best represent local-scale velocity structure in southwest Montana, rather than broader crustal structure across all western Montana.

The 2005 seismic velocity model improved upon prior models in part due to reliability testing, which can help to quantify the robustness of the model. Zeiler et al. (2005) used the new velocity model to determine the hypocenter locations of 14 known mining blasts in southwest Montana. Blast epicenters located with the derived velocity model were compared with the known positions of the mining blasts. Out of the 14 mining blasts, 11 were located within 3 km or less of the true location. These uncertainties are relatively large, partly because of small blast magnitudes and sparse seismographic coverage at the time. Given the marked improvements in seismic monitoring equipment and regional network density, this is an opportune time to develop an updated velocity model.

Depth (km)	2005 Model	1997 Model	1984 Model
0	5.70 km/s	5.52 km/s	4.80 km/s
1.1			5.60 km/s
5.9		6.12 km/s	
6.5			6.15 km/s
7	6.12 km/s		
18			6.80 km/s
18.6		6.74 km/s	
19.8	6.53 km/s		
38.7		8.00 km/s	
39.7	8.0 km/s		
40			8.0 km/s

Table 1*. Comparison of three seismic velocity models derived for southwestern Montana in 1984, 1997, and 2005. The seismic velocities represent P-wave velocities (km/s) for*

layer-interface depths below the local average elevation of earth's surface. Note that the depth increments are not uniform.

Two factors that have hindered the development of high-resolution, accurate, and widespread seismic velocity models for western Montana are: (1) limitations in seismic-network density and sensitivity, and (2) a lack of naturally occurring, high-magnitude events. The new seismic velocity models presented here have benefited from developments on both fronts. Seismic networks in Montana have continued to improve and expand, particularly with the addition of digital broadband sensors to the MRSN, the inception of the new University of Montana Seismic Network (UMSN) in 2017, and the temporary installation of USArray Transportable Array (TA) stations in Montana from c. 2006-2009. Furthermore, a relatively large earthquake (M5.8) struck west-central Montana near the town of Lincoln in 2017 and generated a robust aftershock sequence (McMahon et al., 2019; Smith et al., 2021; Stickney, 2022).

1.3 The 2017 M5.8 Lincoln Earthquake

On 6 July 2017, a M5.8 earthquake occurred 11 km southeast of Lincoln, Montana at a depth of 12.2 km (McMahon et al. 2019; Smith et al. 2021; Stickney, 2022) and was reported to be felt at epicentral distances of more than 800 km (USGS, 2018). The earthquake ruptured on a north-trending, left-lateral strike-slip fault lacking surface expression (McMahon et al. 2019; Smith et al. 2021).

In the first three weeks after the mainshock, 3005 aftershocks were recorded, the largest being M5. During the first 41 weeks of the aftershock sequence (through 19 April 2018), 47 aftershocks with M3 or larger were observed (McMahon et al. 2019). Smith et al. (2021) expanded upon McMahon et al. (2019) with a two-year study of the Lincoln aftershock sequence and relocated 4110 aftershock hypocenters using the 2005 velocity

model (Zeiler et al., 2005). Smith et al. (2021) determined that most aftershocks occurred on the same fault as the mainshock, but identified several additional clusters located primarily to the west of the mainshock that were also oriented approximately north-south. The neighboring clusters extended up to 15 km west of the mainshock and occurred at depths of about 10-20 km. By the end of 2020, aftershock rates had diminished considerably but were still elevated above background seismicity levels. More than three years of elevated and concentrated seismic activity have provided a wealth of data that we use to constrain the seismic velocity structure of west-central Montana as well as to develop an updated regional-scale seismic velocity model for western Montana.

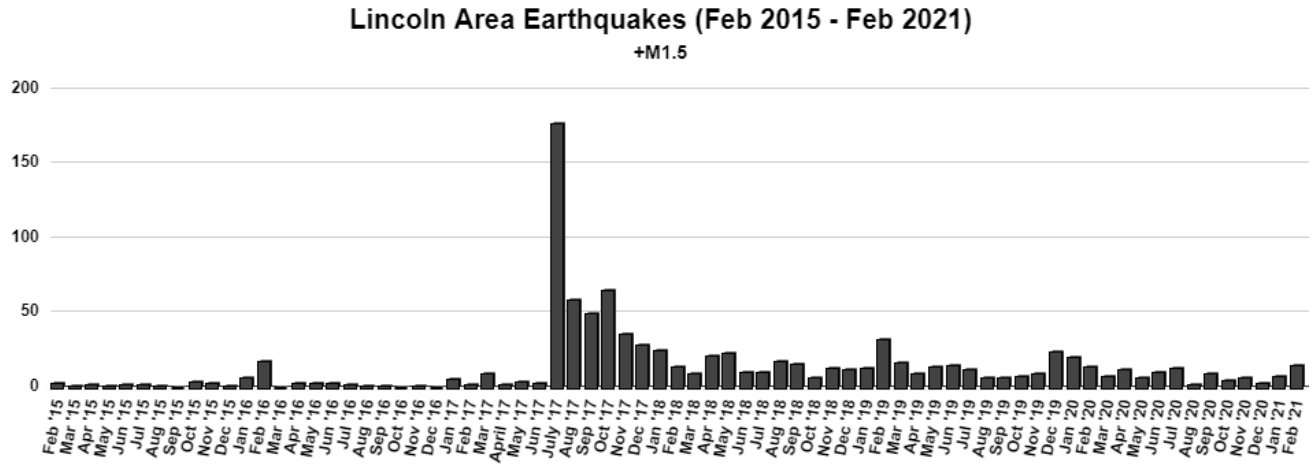

Figure 1. *Monthly number of earthquakes above M 1.5 from February 2015 – February 2021 in the Lincoln area (45°N to 48°N, -114°W to -111°W). The M5.8 Lincoln mainshock occurred on 6 July 2017. The total earthquakes (M1.5+) for this dataset are 1069 events. Data retrieved from the USGS comprehensive earthquake catalog (https://earthquake.usgs.gov/earthquakes/search/).*

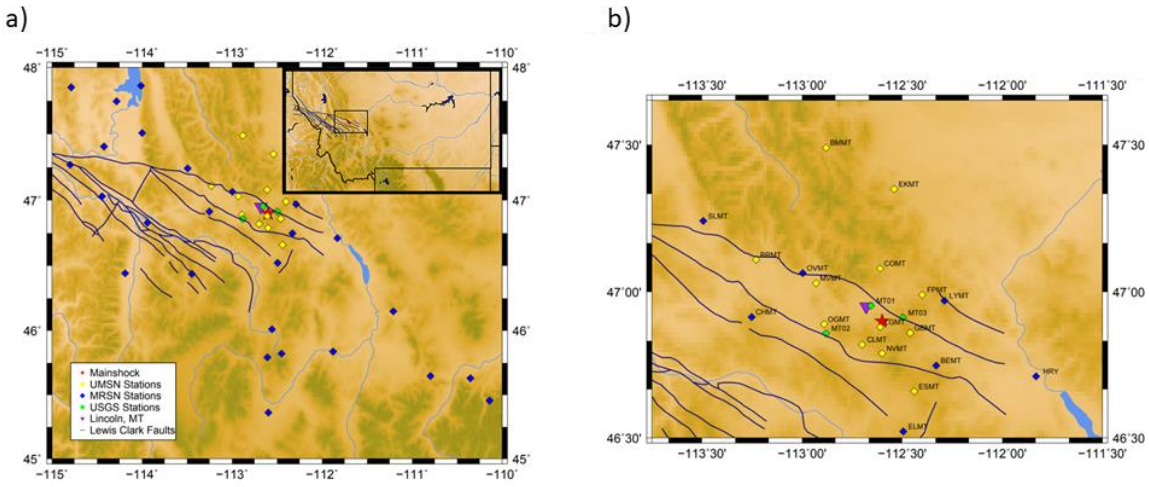

Figure 2. a) *The study region in west-central Montana, including the 2017 mainshock event (red star), relative to the town of Lincoln, Montana (purple inverted triangle), and the three seismic networks used to collect seismic data. Yellow diamonds indicate the locations of the University of Montana Seismic Network seismic stations. Blue diamonds represent the Montana Regional Seismic Network stations, and green diamonds are temporary seismometers installed by the U.S Geological Survey. The Lewis & Clark Line (LCL) faults intersect the study region in blue.* ***b)*** *Enlarged view of* ***Figure 2a*** *to better display individual UMSN and MRSN stations that surround the 2017 mainshock.*

2. Methods

2.1 Seismic Networks Used for Model Derivation

We use continuous seismic data recorded primarily by three seismic networks: the UMSN (Martens & University of Montana, 2017), MRSN (Stickney, 2022), and the USArray TA (e.g., Simpson et al., 2007). UMSN and MRSN data are used to constrain both the local- and regional-scale models. The TA data are used to constrain the regional model.

The UMSN (network code UM) was established in August 2017 to monitor the aftershock sequence of the M5.8 Lincoln earthquake; the first three stations were installed in August 2017, followed by seven additional stations in summer 2018, one station in summer 2019, and one station in summer 2020 (Martens & University of Montana, 2017). All UMSN stations consist of Metrozet MBB-2 broadband, three-

component seismometers with Kinemetrics Obsidian4X digitizers. The stations are deployed strategically around the epicenter of the Lincoln mainshock to reduce the azimuthal gap between stations and thereby provide optimal coverage of the earthquake focal sphere. With waning aftershocks, several stations were decommissioned in summer 2021; three remain active in 2022 (Table 2).

Station	Latitude	Longitude	Elevation (km)	Commission Date	Decommission Date
BMMT	47.4907	-112.8763	1.676	2018-08-22	2021-07-28
BRMT	47.1055	-113.2277	1.388	2020-07-28	Active
CLMT	46.8187	-112.6988	1.616	2018-08-21	2021-07-29
COMT	47.0788	-112.6144	1.665	2018-08-23	Active
EKMT	47.3505	-112.5383	1.473	2018-08-23	2021-07-28
ESMT	46.6567	-112.4426	1.742	2018-08-21	2021-07-29
FPMT	46.9988	-112.4026	1.660	2018-08-23	2021-07-28
GBMT	46.8592	-112.4568	2.235	2017-08-24	2020-07-30
LGMT	46.8813	-112.6051	1.784	2017-08-24	2021-07-27
MVMT	47.0338	-112.9296	1.327	2019-05-07	2021-07-27
NVMT	46.7876	-112.5997	1.741	2017-08-25	2019-04-27
OGMT	46.8864	-112.8878	1.620	2018-08-24	Active

Table 2*: UMSN station coordinates, elevation, and commission and decommission dates. Most of the seismic stations were decommissioned in July 2021 in response to decreasing seismic activity in the study region.*

The Montana Bureau of Mines and Geology (MBMG) established the MRSN (network code MB) beginning in 1980, which currently consists of 46 stations (primarily short period vertical with a few 3-component broadband) across western Montana (MBMG, 1982; Stickney, 2022). The MRSN collects telemetered data that is used by the MBMG, USGS, and the University of Utah for routine earthquake location.

For the regional-scale model, we also incorporate data from the USArray TA, which migrated across Montana from September 2006 through October 2010. The three-component broadband seismic stations of the TA were spaced on a roughly 70 km grid,

which provided unprecedented spatial coverage across the contiguous U.S. (Simpson et al., 2007).

The data from the three networks are supplemented by three temporary broadband stations deployed by the USGS within two days of the 2017 Lincoln earthquake. In October 2017, the three temporary stations were removed; however, a fourth telemetered strong-motion sensor was installed in October 2017 at the Lincoln Ranger station and is currently in operation. We also include data recorded by five three-component broadband stations from the Advanced National Seismic System (ANSS) operating in the northern Rocky Mountain region. Together, these networks provide the most comprehensive and highest quality seismic dataset used to date to derive seismic velocity models for Montana.

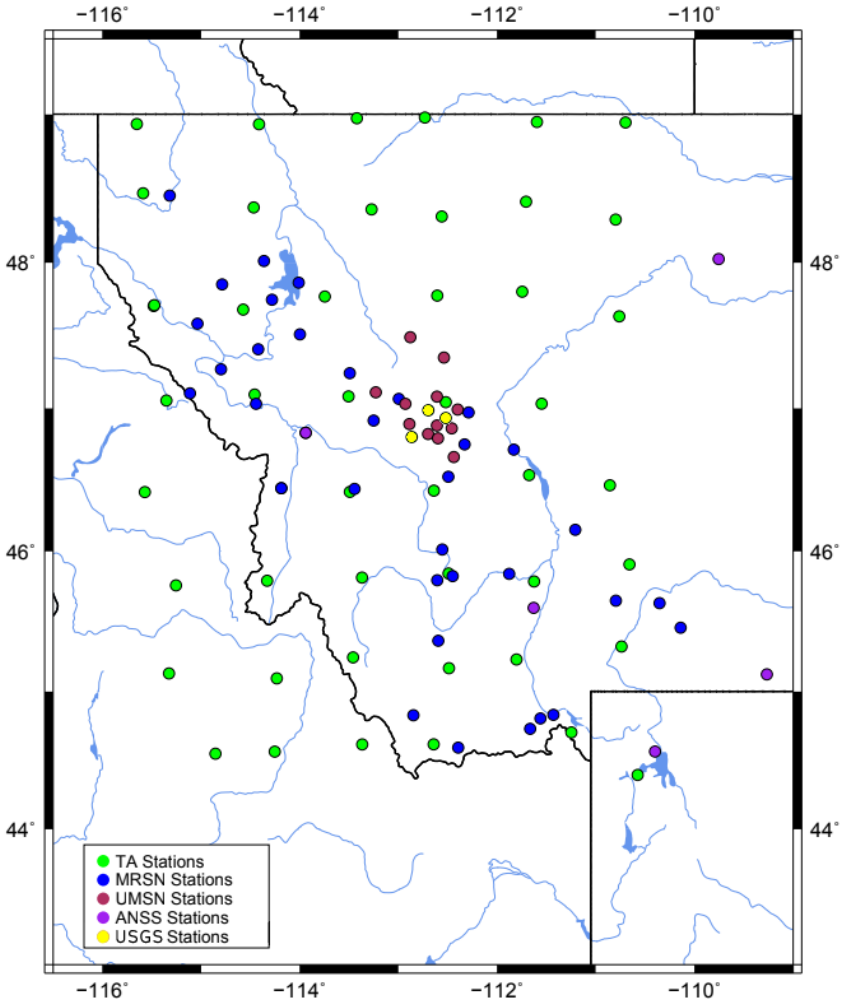

Figure 3. *Locations of the seismic stations used for the local and/or regional model inversions. Green circles represent the USArray TA stations that traversed western Montana from 2006 to 2010. Blue circles represent the Montana Regional Seismic Network. The red circles represent the University of Montana Seismic Network, deployed around the epicenter of the 2017 Lincoln earthquake. Purple circles depict permanent ANSS stations. Yellow circles represent temporary stations the U.S Geological Survey deployed in response to the 2017 Lincoln earthquake.*

2.2 VELEST Software

To estimate the best-fit 1-D seismic velocity models, we use the velocity model inversion software, VELEST, developed by Kissling et al. (1995). The arrival times of the seismic waves represent a nonlinear function of seismic station coordinates, hypocenter positions, and velocity structure. The unknown variables of hypocenter parameters and the velocity structure make the relocation of hypocenters a nonlinear inverse problem. VELEST iteratively determines a linearized solution to the nonlinear-inverse problem in which each iteration simultaneously inverts for hypocenter locations, velocity structure, and station corrections. A least-squares formulation minimizes the differences between predicted and observed seismic arrival times (Kissling et al., 1995). VELEST requires the following as input: a starting velocity model, seismic station coordinates, initial hypocenter locations, and earthquake phase arrivals (both P- and S-wave first arrivals). VELEST accounts for lateral heterogeneities in seismic velocity by way of station corrections.

While VELEST can solve for both P- and S-wave velocity structure jointly, we choose to reduce the number of free parameters and solve solely for the P-wave velocity structure. We constrain the S-wave structure in VELEST with prior, independent knowledge about the V_p/V_s ratio from Smith et al. (2021), who estimated $V_p/V_s = 1.76$ in west-central Montana based on Wadati diagrams (Wadati, 1933).

The Lincoln mainshock-aftershock sequence provides a wealth of data for constraining the shallow structure of west-central Montana; however, the sequence is limited to a relatively small region of western Montana. To better constrain the structure of the deep crust and upper mantle across western Montana for the regional-scale model, we expand the earthquake dataset to include regional events from across western

Montana and east-central Idaho. Furthermore, we also incorporate TA data into the regional-scale model.

2.3 Constraining Local-Scale Velocity Structure in West-Central Montana

To derive the local-scale velocity model for west-central Montana, we rely primarily on earthquake phase arrivals from the Lincoln mainshock-aftershock sequence that occurred within the region of 46.5° - 47.5° N latitude and 112°-114° W longitude. We supplement the dataset with a smaller number of events (167 events) over a broader geographic scope of 45° - 48° N latitude and 111° - 114° W longitude to strengthen constraints on deeper structure. We filtered the events for quality based on the following criteria: 10+ P-wave arrivals, a maximum azimuthal gap of 170°, and a minimum magnitude of 1.0. The total dataset contains 2513 well-recorded earthquakes over a three-year period (July 2017- May 2020). The 2513 events produced 24,380 P-wave arrivals recorded within a maximum epicentral distance of 200 km from the Lincoln mainshock; 93.2% of the earthquakes occur within a 100 km radius of the mainshock.

Nearly all earthquakes in the Lincoln sequence are shallow (< 20 km), which is characteristic of the ISB (Stickney, 2022). The dataset used to constrain the local-scale velocity model contains fewer than 10 events that occurred at depths below 25 km (Figure 9). Therefore, we limit the depth extent of the model to 30 km, which we infer to be above the Moho based on regional studies of seismic-receiver functions (Shen et al., 2013; Mahan et al., 2012, Levander & Miller, 2012; Shen and Ritzwoller, 2016) and previous velocity models (Sheriff and Stickney, 1984; Stickney, 1984; Zeiler, 2005).

Model Region & Earthquake Selection Criteria for West-Central Montana (Local Model)

Model Region & Parameters

1. 45° to 48° N Latitude
2. -114° to -111° W Longitude
3. V_p/V_s Ratio of 1.76

Earthquake Selection Criteria

1. Azimuthal gap of less than 170°
2. Time range July 2017 – May 2020
3. Magnitude of 1.0 or greater
4. 10 or more P wave observations

Totals

Earthquakes: 2513
P-Wave Observations: 24380

Table 3*: Criteria used to select seismic data for the velocity model inversion. Seismic data were collected from the Lincoln mainshock-aftershock sequence in west-central Montana between July 2017 and May 2020 by the UMSN, MRSN, USGS, and ANSS.*

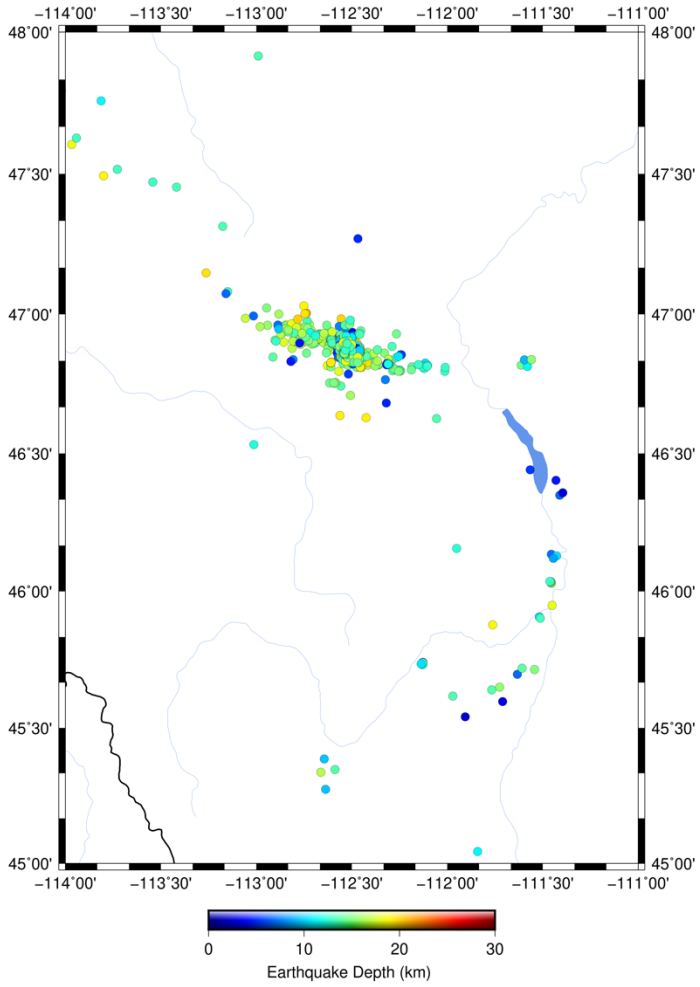

Figure 4. *Location of the 2513 earthquakes used in the inversion for the west-central Montana velocity model. Most events are in the large, central cluster, where the Lincoln mainshock occurred. Events are colored according to depth.*

2.4 Constraining Regional-Scale Velocity Structure in Western Montana

To constrain the velocities of deeper layers over a wider area, we use an expanded dataset of earthquakes from throughout western Montana and east-central Idaho. The dataset consists of earthquakes from 2006-2020, including a small subset of Lincoln aftershocks (102 events above M2.2). We filter the dataset based on a minimum event magnitude of 2.2 and 15+ P-wave observations, as well as an azimuthal gap of less than 170°. The resulting dataset consists of 797 events and 11325 P-wave arrivals recorded within a maximum epicentral distance of 400 km from the center of the study region. By

increasing the maximum epicentral distance to 400 km, we include a broader distribution of seismic stations and earthquakes. The larger earthquake-station distances increase the variety of ray paths that sample deeper structure. We estimate the regional-scale model to a depth of 45 km, which extends into the upper mantle.

Model Region & Earthquake Selection Criteria for Western Montana (Regional Model)

Model Region & Parameters

1. 44° - 49° N Latitude
1. 111° - 116° W Longitude
1. V_p/V_s Ratio of 1.76

Earthquake Selection Criteria

1. Azimuthal gap of less than 170°
1. Time range Sept 2006 – May 2020
1. Magnitude of 2.2 or greater
1. 15 or more P wave observations

Totals

Earthquakes: 797
P-Wave Observations: 11325

Table 4. *Criteria used to select seismic data for the tomographic inversion for the regional velocity model. Seismic data were recorded by the UMSN, MRSN, ANSS and the USArray TA from Sept 2006 to May 2020.*

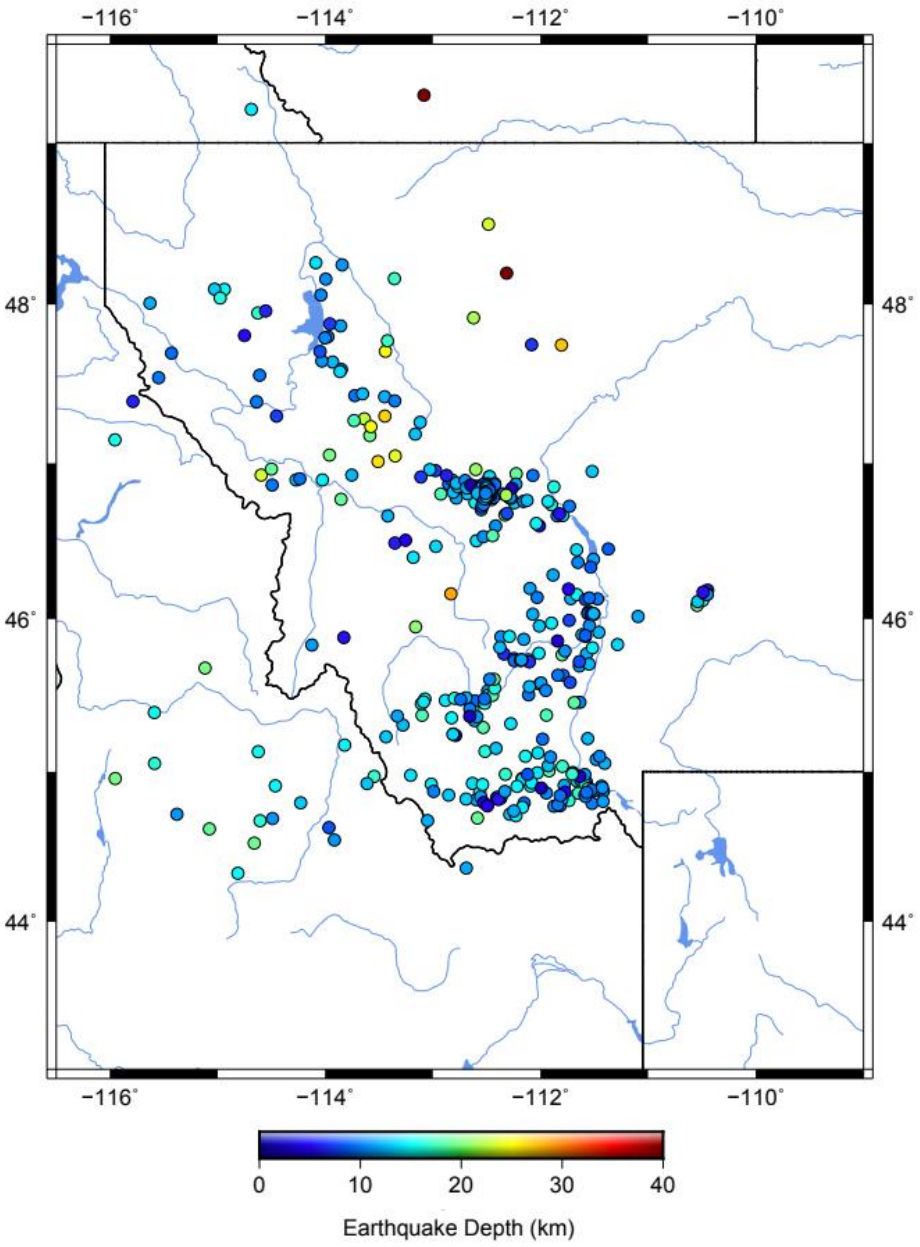

Figure 5. *The spatial distribution of the 797 earthquakes used in the inversion for the regional-scale model. All earthquakes are greater than or equal to M2.2 with 15 or more P-wave observations recorded from September 2006 to May 2020, colored by depth.*

3. Results

3.1 Local-Scale Velocity Model for West-Central Montana

An important component for determining a 1-D seismic velocity model with VELEST is the *a priori* seismic velocity model supplied as input. To explore the model space, we investigate a range of trial models, which span depths of -1.80 to 30 km below sea level. The trial models include: three nine-layered homogenous models, three nine-layered heterogeneous step models, and the Zeiler et al. (2005) model for southwestern Montana (Figure 6), which we also discretize into nine layers to fit the structure of the other six trial models. We adopt this trial-model technique following other seismic studies (e.g., Kaypak and Eyidoğan, 2005; Matrullo et al., 2013; Sevilla et al., 2020). VELEST does not invert for layer thickness; thus, the initial models are structured with 2-km-thick layers near the surface, increasing to 5-km-thick layers at deeper depths. We do not allow low-velocity layers in the solution, as they can introduce instability into the inversion. Furthermore, seismic reflection studies performed in the area have found no conclusive evidence for low-velocity layers in west-central Montana within the crust (Vejmelek and Smithson, 1995; Aki *et al.*, 1976). The stability of the inversion is gauged by the consistency of the output velocity structure, hypocenter locations, and station corrections after each iteration. Once the seismic velocity model, relocated hypocenters, and station corrections no longer vary significantly (here, we assume ± 0.05 km/s, 0.10 km, and 0.02 s, respectively) with subsequent iterations, the solution is considered to have converged (Kissling *et al.*, 1995).

The seven trial models converge to stable solutions after 4-6 inversions, with root-mean-square (rms) travel-time residuals of 0.07-0.11 s. The average of the seven trial model solutions (black line in Figure 6a) is then used as input to a subsequent run of

VELEST. We consider the resulting solution as the preferred 1-D seismic velocity model for west-central Montana (black line in Figure 6b).

The preferred velocity model converges to a stable solution after three iterations of the inversion. The rms time residual for the preferred model is 0.07 s, which represents a reduction of 83.7% from the initial rms time-travel residual of 0.43 s. Relative to the input model, the derived model yields average hypocenter adjustments in latitude, longitude, and depth of 0.032 km, 0.012 km, and 0.059 km, respectively.

We combine neighboring layers of similar seismic velocity (within ± 0.05 km/s), which reduces the preferred local model from nine layers to eight layers. P-wave velocities for the preferred model are shown in Table 5. We assume a V_P/V_S ratio of 1.76.

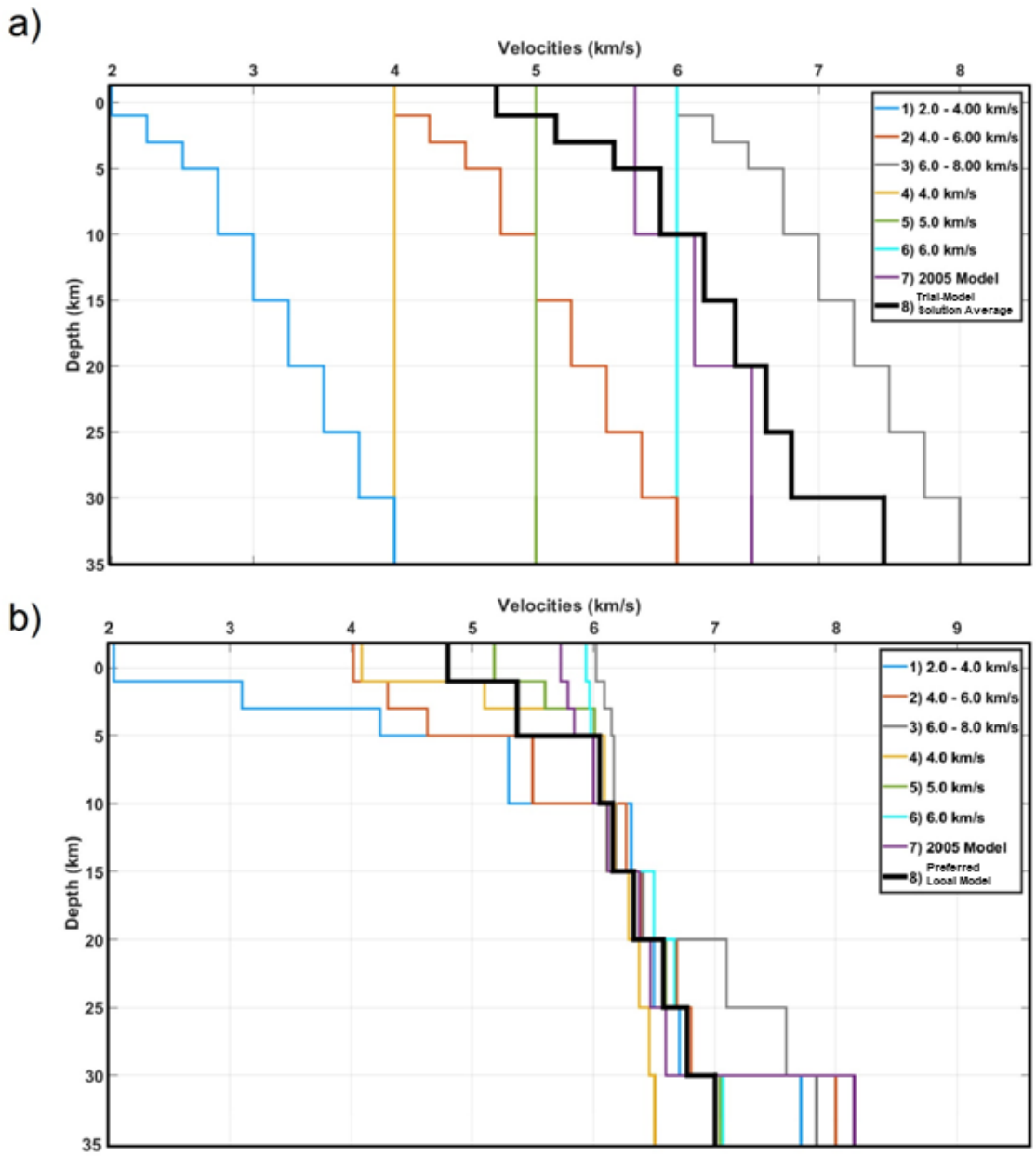

Figure 6. *a) The suite of trial velocity models used as input to VELEST to explore the model space for the local-scale model. Eight initial models labeled in order: models 1-3 consist of nine layers of heterogeneous seismic P-wave velocities, models 4-6 consist of nine layers of homogeneous seismic P-wave velocities, and model 7 is the discretized 4-layered velocity model from Zeiler et al. (2005). Only three of the four layers of the 2005 model are represented here, as we explore structure down to 30 km whereas the 2005 model extends to 40 km. The trial model solution average (black line, model 8) is calculated from the mean of the final outputs for the first seven starting models (Figure 6b).* ***b)*** *Seismic velocity-model solutions derived from the eight trial models in 6a.*

The preferred local-scale model has a near-surface velocity of 4.80 km/s, mid-crustal velocities between 6.05 and 6.77 km/s from 3.0–25.0 km depth, and a deep-crustal

velocity of 7.00 km/s at 30 km depth (Table 5). The consistency of model solutions in Figure 6b suggests that the local-scale velocity model is best constrained within the mid-crust, where most of the earthquakes occurred. Despite differences in layer thicknesses and depths, the mid- and deep-crustal velocities are consistent with Zeiler et al. (2005), indicating that west-central and southwestern Montana may have similar mid- and deep-crustal velocity structure. The preferred local model for the west-central region also exhibits similarities to the results of Zeiler et al. (2005) in the uppermost crust (5.37 km/s at 1 km vs 5.70 km/s at 0 km, respectively), suggesting consistencies in general upper-crust structure across western Montana.

We test the resolution and stability of the preferred local velocity model by randomly perturbing the initial hypocenter locations by up to ± 2.0 km in the model space before performing a subsequent inversion, as suggested by Kissling et al. (1995). When the velocity-model solution is robust, we expect the randomly perturbed hypocenter locations to return to their original input locations within a threshold (here, we assume less than ± 0.5 km).

This process yields stable hypocenter locations for all but 55 of the 2513 hypocenters (~ 2.2%). We find that the outlying events are located at greater distances from the center of the study region and/or had limited phase picks relative to other earthquakes in the dataset. We also find that the station corrections and velocity structure remain stable during the testing process.

3.2 Estimation of Uncertainties for the Local-Scale Velocity Model

Using the trial model solution average as input (black line, Figure 6a) and identical VELEST parameter settings used to determine the local seismic velocity model

for west-central Montana, we generate a suite of 100 new solutions for velocity structure by randomly selecting a sample of 2000 earthquakes from the full dataset of 2513 earthquakes (i.e., 80% of the full dataset) for each run of the inversion. The distribution of the resulting velocity models is shown in Figure 7b. From this distribution, we compute the standard deviation for each layer velocity, which provides an estimate of the precision and uncertainty in the estimated P-wave velocity at each depth. We find small uncertainty values (between ± 0.02 km/s and ± 0.09 km/s) from depths of 10 km to 30 km below sea level. The greatest uncertainty of ± 0.14 km/s corresponds to near-surface structure at 1 km depth. Layers 12 km to 17 km deep are best constrained because most earthquakes ruptured in this depth range. Table 5 provides the 1-σ standard deviation for each layer.

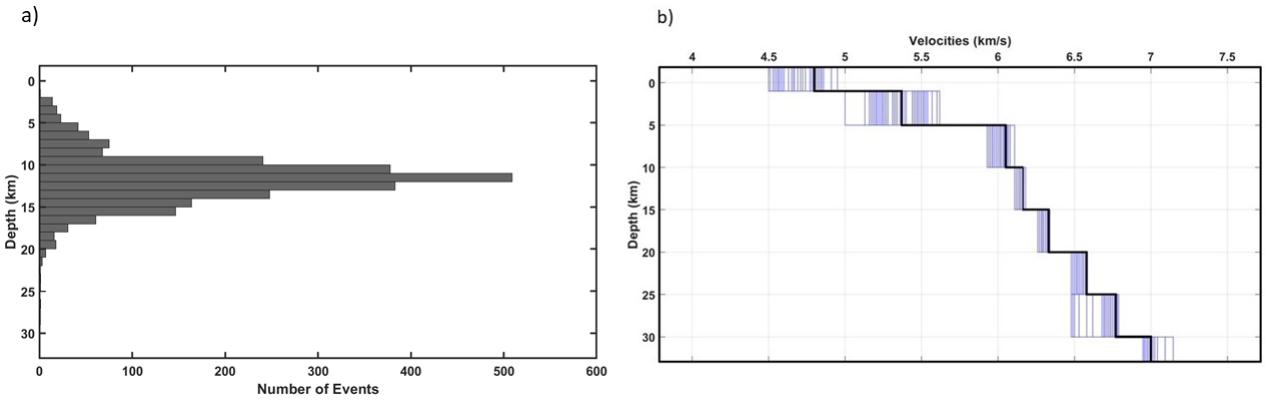

Figure 7. a) *Distribution of hypocenter depths for the 2513 earthquakes used in the inversion for local structure in the Lincoln region of west-central Montana. Most earthquakes occur at mid-crustal depths of about 12-17 km.* ***b)*** *Distribution of 100 velocity models derived from random subsets of the total catalog of 2513 earthquakes. The black line depicts the preferred local-scale velocity model.*

3.3 Station Corrections for the Local-Scale Velocity Model

When using 1-D velocity models, station corrections can help account for 3-D variations in velocity structure near individual seismic stations (Pujol, 1988 and Viret et

al., 1984). Because VELEST does not resolve lateral variations in velocity structure, station corrections can prove especially useful in areas such as west-central Montana where previous tectonic and volcanic activity have resulted in a complex geological framework and lateral structural variations (Prodehl et al., 1989; Portner et al., 2011; Melson, 1971).

The station corrections calculated in VELEST represent average time delays relative to the near surface velocities in the preferred local-scale model (Kissling et al, 1995). The seismic stations in the west-central region are spread across a range of elevations from 1.3 km to 2.4 km above sea level, with an average network elevation of 1.80 km. For seismic stations in west-central Montana, we hold the preferred local-scale velocity model and hypocenter locations fixed in the inversion for station corrections. Station corrections range from –0.63 s to 0.69 s.

Figure 8 shows calculated station corrections. The spatial distribution of positive (late) and negative (early) values corresponds to low and high relative velocities in the vicinity of each seismic station. We primarily find positive station corrections at higher elevations (above 1.8 km), which is expected due to the longer ray paths. Table S1 in the supporting information lists the corrections for each station.

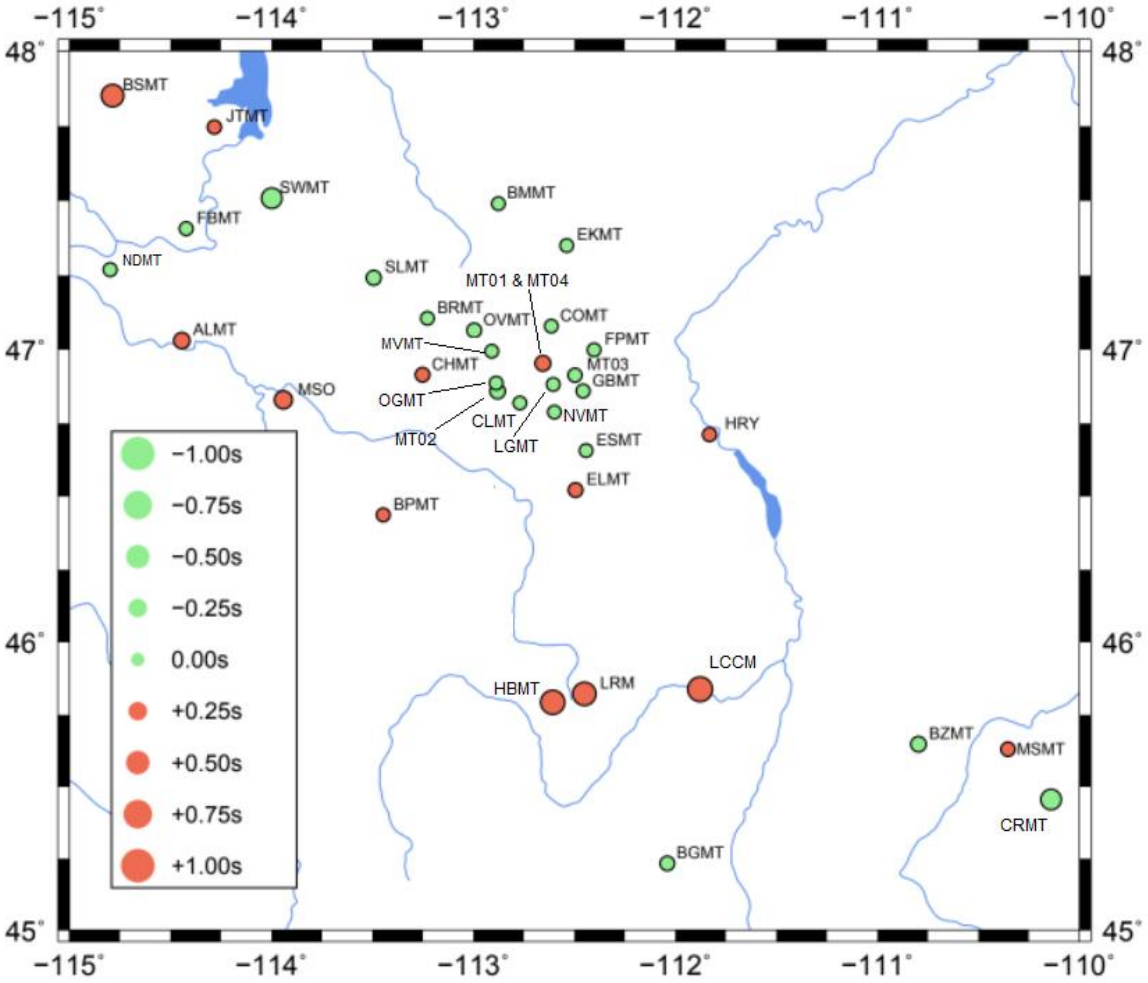

Figure 8. *Station corrections, in seconds, determined by the inversion of P-wave arrivals while holding the velocity model and hypocenter locations fixed. Each station is scaled by its estimated station correction. We show only those seismic stations in the Lincoln region of west-central Montana (UMSN, USGS, and MRSN). Idaho and Wyoming stations are excluded.*

3.4 Regional-Scale Velocity Model for Western Montana

Using the same strategy as for the local-scale velocity model, we design a set of seven trial models to explore the model space for the regional-scale velocity model. The trial models extend to 45 km depth and contain fifteen layers, with 2-km resolution intervals in the upper crust, decreasing to 5-km spacing in the mid crust, and increasing to 2.5-km spacing in the lower crust and upper mantle to better capture the Moho. Each trial model converges to a stable solution after 7-9 iterations, with rms travel-time residuals of

0.40-0.42 s. The travel-time residuals for the regional-scale models are several-fold larger than for the local-scale models, likely due to a larger geographical extent (and more lateral heterogeneities in structure), deeper ray paths, fewer earthquakes in the catalog, and a broader network distribution.

An average of the solutions from the trial models is then used as an input model for a subsequent run of VELEST. The resulting solution is the preferred model for regional-scale velocity structure across western Montana. We again assume a Vp/Vs ratio of 1.76. The preferred regional model reached a stable solution after three iterations with a rms time residual of 0.40 s, which represents a reduction of 68.5% from the residual for the first iteration of the inversion (1.27 s), and with average latitude, longitude, and depth adjustments of 0.037 km, 0.045 km, and 0.140 km, respectively. Combining neighboring layers with similar seismic velocities (within ± 0.05 km/s) reduces the preferred model to thirteen layers, spanning from 1.80 km above sea level to 45 km below sea level.

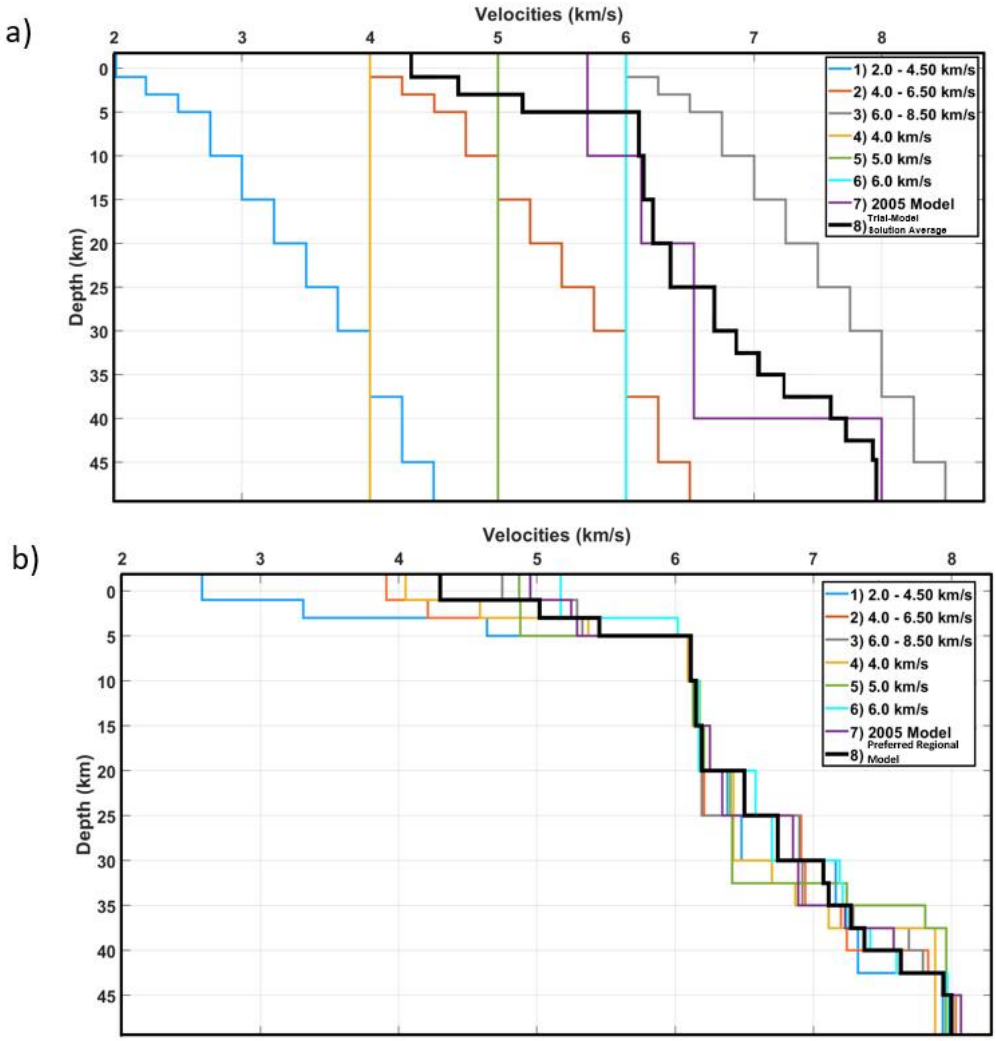

Figure 9. a) *The suite of trial models used as input to VELEST for exploring the regional structure of western Montana. Eight trial models are labeled in order: models 1-3 display a fifteen-layer heterogeneous structure, models 4-6 display a fifteen-layer homogeneous velocity structure, and model 7 is the 4-layered velocity model from Zeiler et al. (2005), which has been discretized to 15 layers to remain consistent with the first six models. The trial model solution average (black line, model 8) is calculated from the mean of the outputs for the seven starting models (Figure 9b).* ***b)*** *Velocity model solutions derived from the eight trial models in Figure 9a.*

The preferred regional-scale model has a near-surface velocity of 4.30 km/s, increasing to 5.45 km/s at 3 km depth, and 6.11-7.07 km/s at mid-crustal depths. At 35 km depth, we estimate a seismic velocity of 7.27 km/s, which increases to 8.00 km/s below 45 km depth (Table 5). Independent receiver-function studies have placed the

Moho in western Montana at roughly 35-40 km depth (Shen et al., 2013; Mahan et al., 2012, Levander & Miller, 2012; Shen and Ritzwoller, 2016). Although our tomographic results do not clearly delineate the Moho boundary, the seismic velocities below about 35-40 km depths are consistent with upper-most mantle velocities.

Compared with the local-scale model for west-central Montana, the near-surface velocity for the regional-scale model is somewhat slower (4.30 km/s vs 4.80 km/s). The near-surface velocity is also slower than the near-surface velocity of 5.70 km/s derived by Zeiler et al. (2005) for southwestern Montana. We attribute the differences largely to discrepancies in layer thicknesses for near-surface layers between the older models and the model presented here. The older models had thicker near-surface layers and therefore represented more of an upper-crust average. Indeed, we also find velocities >5 km/s at 1 km depth below sea level. Furthermore, lateral variations in shallow structure across the broader region, as well as weaker constraints on near-surface structure when performing a regional-scale inversion, can account for differences in near-surface velocity structure. By incorporating longer ray paths into the inversion, we better constrain deeper structure but lose resolution of shallower layers, especially where there are regional-scale lateral contrasts in shallow structure. Local-scale models are constrained by shorter event-station distances than the regional-scale models.

We further tested the resolution and stability of the preferred regional-scale model by randomly perturbing the initial hypocenter locations by up to ± 2.0 km in the model space before performing a subsequent inversion. When the stability test is performed for the regional-scale model, we find that all but 31 of the 797 hypocenters (approximately 3.89% of the dataset) relocate to within less than ± 0.5 km of their original depths. The 31

outlying events are mostly located at shallower depths (between 0 km and 7 km), which are not as well constrained. We also find that the velocity structure remains stable during the testing process.

3.5 Estimation of Uncertainties for the Regional-Scale Velocity Model

Using the trial model solution average (black line in Figure 9a) as a starting model, as well as the same VELEST parameter settings used to derive the regional-scale model, we generate a suite of 100 new velocity-model solutions. For each inversion, we randomly select 637 earthquakes from the full dataset of 797 earthquakes (i.e., 80% of the full dataset). From the distribution of velocities in each layer for the 100 solutions, we compute the standard deviation from the mean, which provides an estimate of uncertainty for the inferred velocity in each layer. The tightest constraints are found at depths between 5 km and 20 km below sea level, which corresponds to the lowest uncertainties of ± 0.01 km/s to ± 0.08 km/s. The well-resolved layers are constrained by the high number of earthquakes that rupture at depths of about 7 km to 17 km (Figure 10a). We also estimate relatively small uncertainties (± 0.04 km/s) in the upper mantle. The greatest uncertainties correspond to near-surface layers at depths of 1 km and 3 km below sea level, with ± 0.26 km/s and ± 0.21 km/s, respectively. Table 5 provides uncertainty estimates for each layer.

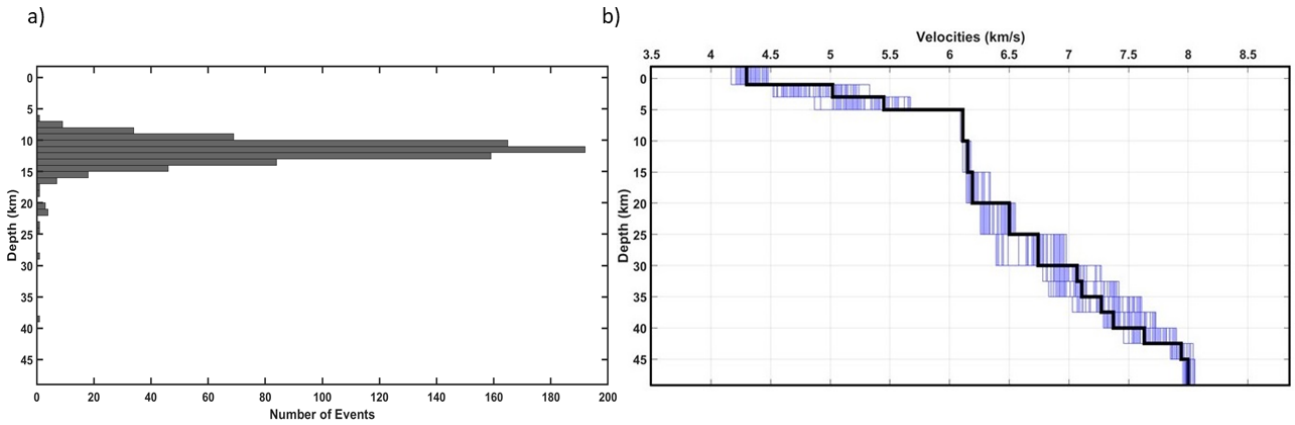

Figure 10. a) *Distribution of hypocenter depths for the 797 earthquakes used in the inversion for the regional-scale velocity structure of western Montana. Most earthquakes occur at mid-crustal depths of about 7-17 km with a small fraction occurring deeper than 20.0 km.* ***b)*** *Distribution of one-hundred velocity models derived from random subsets of earthquakes selected from the catalog of 797 events across western Montana. The black line represents the preferred regional-scale velocity model.*

4. Discussion

4.1 Comparison with Previous Velocity Models for western Montana

The preferred local- and regional-scale models for west-central and western Montana are broadly consistent with prior velocity models that focused on southwest Montana (Sheriff & Stickney, 1984; Stickney, 1997; Zeiler et al., 2005). Near-surface velocities in the prior three models average 5.60 km/s. The local-scale and regional-scale models derived here exhibit a P-wave velocities of 4.80 km/s and 4.30 km/s, respectively, in the upper-most layers, which increase to greater than 5.0 km/s by 1 km depth and greater than 6.0 km/s by 5 km depth. We note that the 2005 model agrees well with the local-scale model, suggesting that west-central Montana and southwest Montana may have similar near-surface and mid-crustal velocity structures.

At mid-crustal depths (~6-20 km), previous models for southwest Montana show similar velocities of 6.12-6.74 km/s; we find similar mid-crustal velocities for west-central and western Montana as well (6.05-6.58 km/s). We hypothesize that the older and

newer models are likely consistent within error for the mid-crustal ranges as the older models for western Montana did not include uncertainty estimates. As seen in Figures 7 and 10, many of the earthquakes across western Montana rupture between about 7 and 17 km, providing strong constraints within this depth range. Subtle differences between the models may also be due to lateral variations in velocity structure across western Montana.

Regarding upper-mantle structure, the preferred regional model presented here exhibits a reasonable upper mantle P-wave velocity of 7.94 km/s at 42.5 km depth, which then increases to a velocity of 8.00 km/s below 45 km depth. The estimated 8.00 km/s at 45 km depth is identical to the 8.00 km/s estimated as the velocity of the lower-most layer at 40 km depth in the three previous velocity models.

A distinguishing characteristic of the two preferred velocity models presented here relative to the three previous velocity models is the depth resolution. Here, we image the west-central region of Montana at a depth resolution of 5 km or better to a depth of 30 km and the western region at a depth resolution of 5 km or better to a depth of 45 km. The three previous models extend to a depth of 40 km with a depth resolution of about 5-20 km depending on the layer. While our regional model uses fewer earthquakes than the 2005 model (797 earthquakes compared to 1432 earthquakes), we select only the highest-quality events (M2.2+) and use seismic data from more sophisticated, modern instruments (TA, UM, expanded MB networks). Furthermore, we consider a broader geographic region across western Montana. Comparatively, the earthquakes used to constrain the 2005 model were primarily recorded in east-central Idaho and southwest Montana, biasing the 2005 model to this region.

Depth (km)	2022 West-Central Montana Model (this study)	2022 Western Montana Model (this study)	2005 Southwest Montana Model (Zeiler et al.)	1997 Southwest Montana Model (Stickney)	1984 Southwest Montana Model (Sheriff and Stickney)
-1.8	4.80 km/s ± 0.12 km/s	4.30 km/s ± 0.17 km/s			
0			5.7 km/s	5.52 km/s	4.8 km/s
1	5.37 km/s ± 0.14 km/s	5.02 km/s ± 0.26 km/s			5.6 km/s
3		5.45 km/s ± 0.21 km/s			
5	6.05 km/s ± 0.14 km/s	6.11 km/s ± 0.01 km/s			
5.9				6.12 km/s	
6.5					6.15 km/s
7			6.12 km/s		
10	6.16 km/s ± 0.02 km/s				
15	6.33 km/s ± 0.02 km/s	6.19 km/s ± 0.04 km/s			
18					6.8 km/s
18.6				6.74 km/s	
19.8			6.53 km/s		
20	6.58 km/s ± 0.04 km/s	6.50 km/s ± 0.08 km/s			
25	6.77 km/s ± 0.09 km/s	6.74 km/s ± 0.17 km/s			
30	7.00 km/s ± 0.05 km/s	7.07 km/s ± 0.13 km/s			
32.5					
35		7.27 km/s ± 0.14 km/s			
37.5		7.37 km/s ± 0.14 km/s			
38.7				8.0 km/s	
39.7			8.0 km/s		
40		7.63 km/s ± 0.10 km/s			8.0 km/s
42.5		7.94 km/s ± 0.04 km/s			
45		8.00 km/s ± 0.04 km/s			

Table 5. *Seismic velocity models derived for western Montana. The local-scale model, constrained primarily by Lincoln aftershock data, describes the west-central region of Montana. The regional-scale model, constrained by data across western Montana, represents broader velocity structure across western Montana. The 2005, 1997, and 1984 models are specific to southwest Montana. For the local model, we do not constrain velocity structure for layers deeper than 35 km.*

4.2 Refining Lincoln Aftershock Locations Using the New Local-Scale Model

Using the local-scale velocity model and station corrections derived in this study, we relocate aftershocks from the 2017 Lincoln earthquake with HypoInverse-2000 (Klein, 2002) and HypoDD (Waldhauser and Ellsworth, 2000; Waldhauser, 2001). HypoInverse-2000 processes P- and S-wave phase arrivals, station corrections, and a 1-D seismic velocity model to calculate absolute hypocenter locations. We use the absolute locations as input to HypoDD, which uses a double-difference algorithm to mitigate

travel-time errors that may occur due to lateral heterogeneity in the local seismic velocity structure (Waldhauser and Ellsworth, 2000).

We investigate the extent to which hypocenter locations are adjusted for the Lincoln sequence compared with a prior study by Smith et al (2021), which adopted the 2005 velocity model. For comparison, we use the same earthquake catalog as Smith et al. (2021), which included the P- and S-wave arrivals of earthquakes above M1.0 from 5 July 2017 through 28 April 2019 with a maximum distance of 200 km between cluster centroids and recording seismic stations. Using identical parameters, we then add subsequent earthquakes recorded between 29 April 2019 and 30 May 2020 to explore a third year of the aftershock sequence that has not yet been studied.

Smith et al. (2021) discussed twelve distinct clusters of seismicity located within a 20 km x 15 km area, most with focal depths ranging from 12 to 19 km. The primary cluster, which contains the Lincoln mainshock, features diffuse seismicity that sharpened over time as new UM stations were deployed. Surrounding the primary cluster are several additional clusters that extend across 15 km, mostly to the west of the mainshock. The neighboring clusters align predominantly in the north-south and northeast-southwest directions, parallel to the mainshock fault and oblique to the Lewis & Clark Line faults that traverse the region. With the addition of new seismic data combined with the local-scale velocity model from this study, we identify two additional clusters. Furthermore, the expanded catalog augments previously identified clusters.

Figure 11 shows the previously and newly identified clusters. The new Cluster 13 follows a north-south trend and occurs approximately 7 km west of the mainshock with an average hypocenter depth of ~16 km. The earthquakes in Cluster 13 ruptured between

January 2020 and February 2020. The new Cluster 14 also exhibits a roughly north-south trend and lies about 3 km north-northeast of the mainshock with an average depth of ~9 km and occurred between June 2019 and March 2020.

Many of the cluster geometries retain a similar spatial distribution to that reported in Smith et al. (2021), with sharpening of some clusters with fewer earthquake pairs. Clusters 1, 2 and 8 include additional earthquakes that occurred after 28 April 2019, which is the end of the time range that Smith et al. (2021) analyzed.

Since April 2019, this analysis added 360 additional events to Cluster 1. Cluster 1 still spans roughly the same spatial dimensions (7 x 9 km) as estimated by Smith et al. (2021). With only four events added to Cluster 2 through May 2020, the spatial dimensions of Cluster 2 do not change. Twenty-seven events are added to Cluster 8 through February 2020, resulting in a less sharply defined zone compared to that defined by Smith et al (2021).

a)

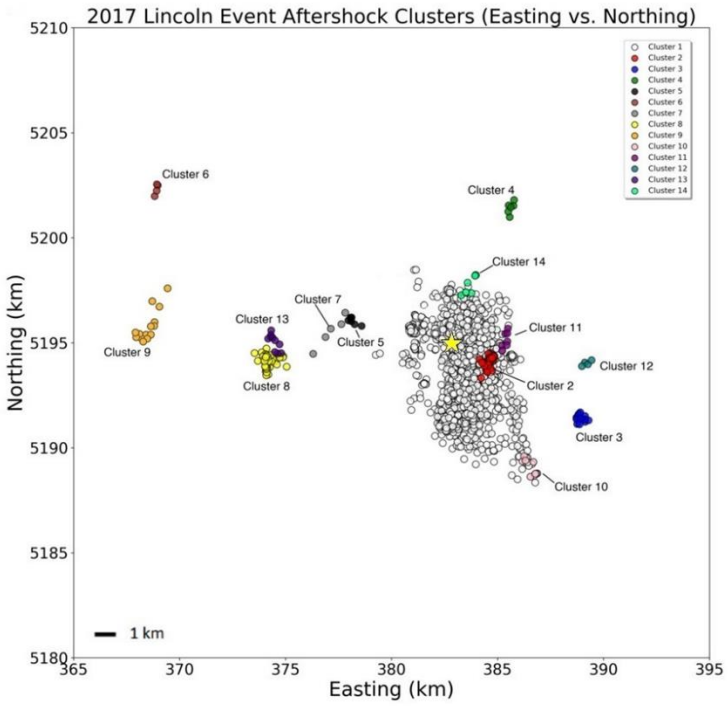
2017 Lincoln Event Aftershock Clusters (Easting vs. Northing)
Northing (km)
Easting (km)
1 km
Cluster 1
Cluster 2
Cluster 3
Cluster 4
Cluster 5
Cluster 6
Cluster 7
Cluster 8
Cluster 9
Cluster 10
Cluster 11
Cluster 12
Cluster 13
Cluster 14

b)

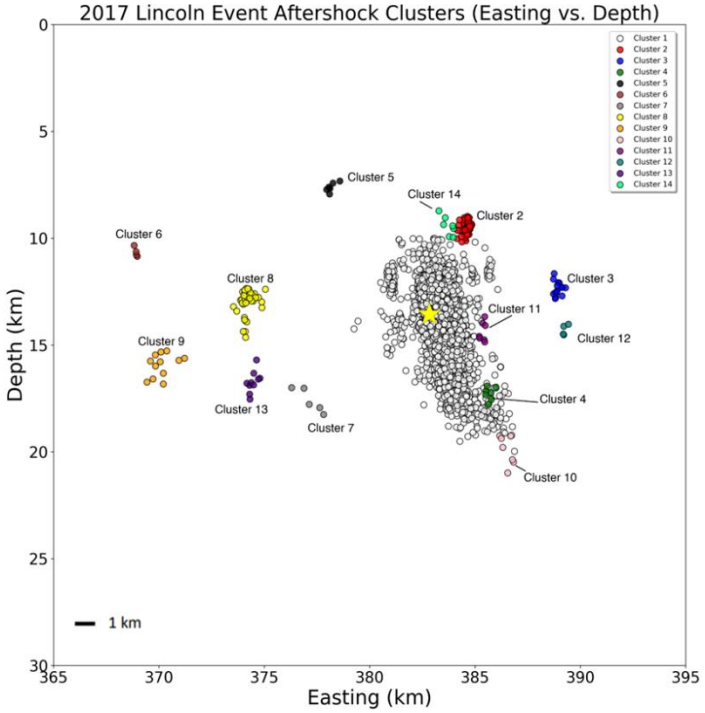
2017 Lincoln Event Aftershock Clusters (Easting vs. Depth)
Depth (km)
Easting (km)
1 km
Cluster 1
Cluster 2
Cluster 3
Cluster 4
Cluster 5
Cluster 6
Cluster 7
Cluster 8
Cluster 9
Cluster 10
Cluster 11
Cluster 12
Cluster 13
Cluster 14

c)

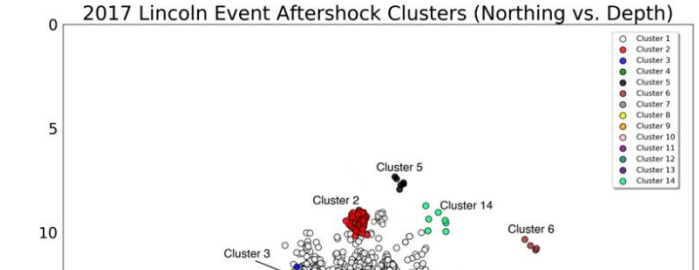
2017 Lincoln Event Aftershock Clusters (Northing vs. Depth)
Cluster 1
Cluster 2
Cluster 3
Cluster 4
Cluster 5
Cluster 6
Cluster 7
Cluster 8
Cluster 9
Cluster 10
Cluster 11
Cluster 12
Cluster 13
Cluster 14

***Figure 11**. **a)** Double-difference relocations for all events (M1+) since the Lincoln mainshock through 30 May 2020, located with the new local-scale model for west-central Montana. Events are color-coded by cluster and plotted in UTM coordinates of easting vs northing (km). The main cluster, shown in white, includes the Lincoln mainshock. Clusters 13 and 14 are newly identified clusters that include earthquakes that occurred between 29 April 2019 and 31 March 2020. **b)** Same as Figure 11.a but showing earthquakes in easting versus depth (km). **c)** Same as Figure 11.a but showing earthquakes in northing versus depth (km).*

Table 6 summarizes the relocated earthquake clusters according to number of events, inferred fault orientation, distance of the cluster from the mainshock, depth range of the hypocenters, and time period. In comparison with Smith et al. (2021), epicentral locations of clusters remain relatively stable. The updated velocity model has the greatest impact on the depth of hypocenters. The depth adjustments could reflect the increased depth resolution of the new model, because the 2005 model consisted of only four layers from 0 km to 40 km depth. Cluster 6 exhibits the greatest change in depth when adopting the new velocity model; approximately 1.5 km. Cluster 6 is located furthest from the mainshock, at 15 km to the northwest, which may explain the larger adjustment. The remaining clusters change by less than ± 1 km relative to the locations reported in Smith et al. (2021).

Cluster	Number of Events	Spatial Area	Trend Direction	Distance from Mainshock	Depth Range	Time Period
1	2537	7.0 km by 9.0 km	N-S	0 km	10-20 km	7/17-5/20
2	71	0.5 km by 1.0 km	NNE-SSW	2 km in depth	8-10 km	7/17-5/20
3	19	0.5 km by 0.3 km	NNE-SSW	7.8 km SE	11-13 km	7/17-10/17
4	5	0.2 km by 0.5 km	N-S	7 km N	15-17 km	5/18-6/18
5	6	0.2 km by 0.2 km	NNW-SSE	5 km W	7-8 km	10/18
6	5	0.2 km by 0.1 km	N-S	15 km NW	10-11 km	4/19

7	5	2.0 km by 2.0 km	NNW-SSE	7 km W	16-18 km	7/17-12/17
8	44	2.0 km by 2.0 km	N-S	12 km W	12-15 km	2/19-2/20
9	13	1.5 km by 2.5 km	N-S	15 km W	15-17 km	7/17-10/17
10	10	0.8 km by 1.0 km	NNW-SSE	5 km SSE	19-21 km	7/17-8/17
11	6	0.2 km by 1.0 km	N-S	5 km E	13-15 km	11/17-5/18
12	4	0.2 km by 0.5 km	NNE-SSW	5 km E	14-16 km	11/18
13	10	1.0 km by 1.5 km	N-S	12 km W	15-18 km	1/20-2/20
14	7	1.0 km by 1.0 km	N-S	4 km N	8-10 km	6/19-3/20

Table 6. *Event counts, inferred fault trend, distance from mainshock, hypocenter depth range, and time period for the primary earthquake clusters in the Lincoln aftershock sequence. We consider events through May 2020.*

4.3 A Note on Moho Depth

Seismic refraction studies have postulated that the Moho discontinuity can be distinguished, albeit not sharply defined, by P-wave velocities increasing gradually from a range of 6.5 km/s – 7.1 km/s to a range of 7.6 km/s – 8.0 km/s (Jarchow and Thompson, 1989; Christensen and Mooney, 1995; Carbonell et al., 2013). The roughly 6.5-8.0 km/s velocity transition occurs at depths of about 20-70 km in continental crust, depending on the geographic location (Laske et al., 2013; Carbonell *et al.*, 2013). For the western Montana region, multiple seismic receiver-function studies have estimated the local crustal thickness to be between about 35-40 km (e.g., Shen et al., 2013; Mahan et al., 2012, Levander & Miller, 2012; Shen and Ritzwoller, 2016). The variable range of 35-40 km is attributed to the complex tectonic history of western Montana, lateral variations in Moho depth across the region, and uncertainties in the receiver-function data and analysis.

To better image the crust-mantle interface, we increase depth resolution to 2.5 km below 30 km depth in the regional-scale model; 2.5 km provides a balance between depth resolution and stability (i.e., the number of free parameters in the model). Our preferred regional-scale model exhibits a gradual increase in P-wave velocity from 7.1 km/s to 7.6 km/s between depths of 30 km and 40 km. Although the Moho boundary is not sharply defined, the results are consistent with independent receiver-function studies that report a Moho depth for western Montana in the range of 35-40 km. Furthermore, the regional-scale model is consistent with Buehler & Shearer (2010), who estimated a large-scale average upper-mantle P-wave velocity across the broader western United States to be 7.93 km/s, with areas of higher P-wave velocities of approximately 8.10 km/s reported in western Montana (Buehler and Shearer, 2014 and 2017). While receiver functions provide an independent estimation of Moho depth, we consider the regional-scale velocity model proposed here to provide a robust representation of velocity structure in western Montana due to the spatially targeted nature of our study.

5. Conclusion

Western Montana is a seismically active region that has undergone multiple tectonic events, resulting in complex structural geology. However, due to infrequent large-magnitude earthquakes in recent decades (only four M5+ events since 1980) and limitations in earthquake-monitoring infrastructure, acquiring high-quality seismic data to place better constraints on seismic velocity structure has been a challenge. Here, we use continuous seismic data from the UMSN, MRSN, and TA, supplemented by data from the USGS and ANSS, to derive new 1-D seismic velocity models for west-central Montana and broader western Montana at unprecedented depth resolution. The new local-

and regional-scale velocity models can improve earthquake hypocenter locations for western Montana, provide better constraints on earthquake focal mechanisms, and advance understanding of regional lithology.

We use seismic datasets collected by several networks to constrain the local- and regional-scale models presented here. The datasets represent the most comprehensive and highest quality datasets used to constrain western-Montana velocity structure to date. The local-scale model for west-central Montana is constrained by 2513 well-recorded earthquakes and 24,380 unique P-wave observations, primarily from the Lincoln mainshock-aftershock sequence. The regional-scale velocity model is constrained by 797 earthquakes and 11,325 unique P-wave observations and provides information on lower crust and upper mantle structure. While fewer earthquakes are used to constrain the regional-scale model relative to the model of Zeiler et al. (2005), the broader distribution (across western Montana) and quality (M2.2+, improved instrumentation) of the earthquake catalog adopted here provide new and robust insights into western-Montana velocity structure. For both the local- and regional-scale models, we assume a V_p/V_s ratio of 1.76 based on the independent Wadati analysis of Smith et al. (2021).

The new models are consistent with prior velocity models for southwestern Montana (e.g., Stickney 1997; Zeiler et al., 2005) as well as with a large-scale seismic tomography study for the western United States (Buehler and Shearer 2010). Minor differences in velocity structure are likely due to regional variations in lithology as well as uncertainties in the tomographic estimates of seismic velocity. We recommend that future analyses of earthquakes in western Montana, and west-central Montana in particular, adopt the new velocity models.

REFERENCES

Aki, K., Christoffersson, A., & Husebye, E. S. (1976). Three-dimensional seismic structure of the lithosphere under Montana LASA. Bulletin of the Seismological Society of America, 66(2), 501-524.

Buehler, J. S., and Shearer, P. M. (2010), Pn tomography of the western United States using US Array, J. Geophys. Res., 115, B09315.

Buehler, J. S., and Shearer, P. M. (2014), Anisotropy and Vp/Vs in the uppermost mantle beneath the western United States from joint analysis of Pn and Sn phases, J. Geophys. Res. Solid Earth, 119, 1200– 1219.

Buehler, J. S., and Shearer, P. M. (2017), Uppermost mantle seismic velocity structure beneath US Array, J. Geophys. Res. Solid Earth, 122, 436– 448.

Carbonell, R., Levander, A., & Kind, R. (2013). The Mohorovičić discontinuity beneath the continental crust: An overview of seismic constraints. Tectonophysics, 609, 353-376.

Christensen, N. I., & Mooney, W. D. (1995). Seismic velocity structure and composition of the continental crust: A global view. Journal of Geophysical Research: Solid Earth, 100(B6), 9761-9788.

Doser, D.I. (1989) Source parameters of Montana earthquakes (1925-1964) and tectonic deformation in the northern Intermountain Seismic Belt: Bulletin of the Seismological Society of America, v. 79, no. 1, pp. 31-50.

Ellsworth, W. L. (1978). Three-dimensional structure of the crust and mantle beneath the island of Hawaii (Doctoral dissertation, Massachusetts Institute of Technology).

Farrell, J. (2019). 60 years since the 1959 M7.3 Hebgen Lake earthquake: its history and effects on the Yellowstone region. USGS, Yellowstone Volcano Observatory.

Farrell, J. M. (2013). Seismicity and tomographic imaging of the Yellowstone crustal magmatic-tectonic system (Doctoral dissertation, The University of Utah).

Jarchow, C. M., & Thompson, G. A. (1989). The nature of the Mohorovicic discontinuity. Annual Review of Earth and Planetary Sciences, 17(1), 475-506.

Kaypak, B., & Eyidoğan, H. (2005). One-dimensional crustal structure of the Erzincan basin, Eastern Turkey and relocations of the 1992 Erzincan earthquake (Ms= 6.8) aftershock sequence. Physics of the Earth and Planetary Interiors, 151(1-2), 1-20.

Kissling, E. (1988), Geotomography with local earthquake data, Rev. Geophys., 26(4), 659–698

Kissling, E., Ellsworth, W. L., Eberhart-Phillips, D., & Kradolfer, U. (1994). Initial reference models in local earthquake tomography. Journal of Geophysical Research: Solid Earth, 99(B10), 19635-19646.

Kissling, E., Kradolfer, U., & Maurer, H. (1995). Program VELEST user's guide-Short Introduction. Institute of Geophysics, ETH Zurich.

Klein, F. W. (2002). User's guide to HYPOINVERSE-2000, a Fortran program to solve for earthquake locations and magnitudes (No. 2002-171). US Geological Survey.

Levander, A., & Miller, M. S. (2012). Evolutionary aspects of lithosphere discontinuity structure in the western US. Geochemistry, Geophysics, Geosystems, 13(7).

Mahan, K. H., Schulte-Pelkum, V., Blackburn, T. J., Bowring, S. A., & Dudas, F. O. (2012). Seismic structure and lithospheric rheology from deep crustal xenoliths, central Montana, USA. Geochemistry, Geophysics, Geosystems, 13(10).

Martens, H.R., & University Of Montana. (2017). University of Montana Seismic Network [Data set]. International Federation of Digital Seismograph Networks. https://doi.org/10.7914/SN/UM

Mason, D. B. (1996). Earthquake magnitude potential of the Intermountain seismic belt, USA, from surface-parameter scaling of late Quaternary faults. Bulletin of the Seismological Society of America, 86(5), 1487-1506.

MATLAB. (2018). 9.7.0.1190202 (R2019b). Natick, Massachusetts: The MathWorks Inc.

Matrullo, E., De Matteis, R., Satriano, C., Amoroso, O., & Zollo, A. (2013). An improved 1-D seismic velocity model for seismological studies in the Campania–Lucania region (Southern Italy). Geophysical Journal International, 195(1), 460-473.

McMahon, N. D., Yeck, W. L., Stickney, M. C., Aster, R. C., Martens, H. R., & Benz, H.M (2019). Spatiotemporal analysis of the foreshock–mainshock–aftershock sequence of the 6 July 2017 M w 5.8 Lincoln, Montana, earthquake. Seismological Research Letters, 90(1), 131–139.

Melson, W. G. (1971). Geology of the Lincoln Area, Lewis and Clark County, Montana. Smithsonian Contributions to the Earth Sciences.

Montana Bureau of Mines and Geology/Montana Tech (MBMG, MT USA). (1982). Montana Regional Seismic Network [Data set]. International Federation of Digital Seismograph Networks.

Laske, G., Masters, G., Ma, Z., & Pasyanos, M. (2013, April). Update on CRUST1. 0—A 1-degree global model of Earth's crust. In Geophys. res. abstr (Vol. 15, p. 2658).

Pavlis, G. L., & Booker, J. R. (1980). The mixed discrete-continuous inverse problem: Application to the simultaneous determination of earthquake hypocenters and velocity structure. Journal of Geophysical Research: Solid Earth, 85(B9), 4801-4810.

Portner, R. A., Hendrix, M. S., Stalker, J. C., Miggins, D. P., & Sheriff, S. D. (2011). Sedimentary response to orogenic exhumation in the northern Rocky Mountain Basin and Range province, Flint Creek basin, west-central Montana. Canadian Journal of Earth Sciences, 48(7), 1131-1154.

Pujol, J. (1988). Comments on the joint determination of hypocenters and station corrections. Bulletin of the Seismological Society of America, 78(3), 1179-1189.

Prodehl, C., Lipman, P. W., Pakiser, L. C., & Mooney, W. D. (1989). Crustal structure of the Rocky Mountain region. Geophysical framework of the continental United States, 172, 249-284.

Roecker, S. W. (1981). Seismicity and tectonics of the Pamir-Hindu Kush region of central Asia (Doctoral dissertation, Massachusetts Institute of Technology).

Rudnick, R. L., Gao, S., Holland, H. D., & Turekian, K. K. (2003). Composition of the continental crust. The crust, 3, 1-64.

Scott, H.W. (1936) The Montana earthquakes of 1935: Montana Bureau of Mines and Geology Memoir 16, p. 47.

Sears, J. W., and M. Hendrix (2004). Lewis and Clark line and the rotational origin of the Alberta and Helena salient, North American Cordillera, in Orogenic Curvature: Integrating Paleomagnetic and Structural Analysis, A. J. Susan and A. B. Weil (Editors), Geol. Soc. Am. Special Paper 383, 173–186

Sevilla, W. I., Jumawan, L. A., Clarito, C. J., Quintia, M. A., Dominguiano, A. A., & Solidum Jr, R. U. (2020). Improved 1D velocity model and deep long-period earthquakes in Kanlaon Volcano, Philippines: Implications for its magmatic system. Journal of Volcanology and Geothermal Research, 393, 106793.

Shen, W., Ritzwoller, M. H., & Schulte-Pelkum, V. (2013). A 3-D model of the crust and uppermost mantle beneath the Central and Western US by joint inversion of receiver functions and surface wave dispersion. Journal of Geophysical Research: Solid Earth, 118(1), 262-276.

Shen, W., & Ritzwoller, M. H. (2016). Crustal and uppermost mantle structure beneath the United States. Journal of Geophysical Research: Solid Earth, 121(6), 4306-4342.

Sheriff, S. D., and M. C. Stickney (1984). Crustal structure of SW Montana and east central Idaho results from a reversed refraction line, Geophys. Lett. Rev. 11, 299–302

Smith, E. M., Martens, H. R., & Stickney, M. C. (2021). Microseismic evidence for bookshelf faulting in western Montana. Seismological Society of America, 92(2A), 802-809.

Smith, R. B., and W. J. Arabasz (1991). Seismicity of the intermountain seismic belt, in Neotectonics of North America, D. B. Slemmons, E. R. Engdahl, M. D. Zoback, and D. D. Blackwell (Editors), Geological Society of America, 185–228.

Spencer, C., & Gubbins, D. (1980). Travel-time inversion for simultaneous earthquake location and velocity structure determination in laterally varying media. Geophysical Journal International, 63(1), 95-116.

Stein, S., & Mazzotti, S. (Eds.). (2007). Continental intraplate earthquakes: science, hazard, and policy issues (Vol. 425). Geological Society of America.

Stickney, M. C. (1984). P-wave travel times and crustal structure of SW Montana from aftershocks of the October 28, 1983, Borah Peak, Idaho, Earthquake, U.S. Geologic Survey, Proceedings of Workshop XXVIII, Vol. A., Open-File Rept. 85-290.

Stickney, M.C., and Bartholomew, M.J., 1987, Seismicity and Quaternary faulting of the northern basin and range province, Montana and Idaho: Bulletin of the Seismological Society of America, v. 77, p. 1602–1625.

Stickney, M. C. (1997). Seismic source zones in southwest Montana, Montana Bureau of Mines and Geology Open-File Rept. 366.

Stickney, M., Haller, K., Machette, M. (2000). Quaternary Faults and Seismicity in Western Montana. Montana Bureau of Mines & Geology. Special Publication No. 114.

Stickney, M. (2015). Seismicity within and adjacent to the eastern Lewis and Clark line, west-central Montana. Northwest Geol., 44, 19-36.

Stickney, M. (2022). Earthquakes and Seismographic Monitoring in Montana. Montana Bureau of Mines & Geology. Geology of Montana, Vol II, Montana Seismicity.

Thurber, C. H. (1981). Earth structure and earthquake locations in the Coyote Lake area, central California (Doctoral dissertation, Massachusetts Institute of Technology).

U.S. Geological Survey (USGS) (2018). M 5.8—11km SE of Lincoln, Montana, available at https://earthquake.usgs.gov/earthquakes/eventpage/us10009757/moment-tensor

Vejmelek, L., & Smithson, S. B. (1995). Seismic reflection profiling in the Boulder batholith, Montana. Geology, 23(9), 811-814.

Viret, M., G. Bollinger, J. Snoke, and J. Dewey (1984). Joint hypocenter relocation studies with sparse data sets--A case history: Virginia earthquakes, Bull. Seism. Soc. Am. 74, 2297-2311.

Wadati, K. (1933). On the travel time of earthquake waves, Part II, Geophys. Mag., 7: 101-111.

Waldhauser, F., & Ellsworth, W. L. (2000). A double-difference earthquake location algorithm: Method and application to the northern Hayward fault, California. Bulletin of the seismological society of America, 90(6), 1353-1368.

Waldhauser, F. (2001). HypoDD -- A Program to Compute Double-Difference Hypocenter Locations, Columbia University.

Wallace, C. A., D. J. Lidke, and R. G. Schmidt (1990). Faults of the central part of the Lewis and Clark line and fragmentation of the Late Cretaceous foreland basin in west-central Montana, Geol. Soc. Am. Bull. 102, no. 8, 1021–1037.

Wessel, P., and W. H. F. Smith (1998), New, improved version of the Generic Mapping Tools released, Eos Trans. AGU, 79, 579–579.

Zeiler, C. P., Stickney, M. C., & Speece, M. A. (2005). Revised velocity structure of western Montana. Bulletin of the Seismological Society of America, 95(2), 759–762.

Supplementary Information

Detailed process of seismic data collection process:

Because the UMSN stations are not telemetered, the data must be manually retrieved and archived. This data retrieval is done approximately every three to nine months, typically during the summer and then again before the winter season. After retrieving data from the seismic stations, they are archived at the Incorporated Research Institutions for Seismology (IRIS) website. The continuous waveform data from the UMSN, as well as other networks such as the MRSN, can be viewed and retrieved from the IRIS website: https://ds.iris.edu/mda/

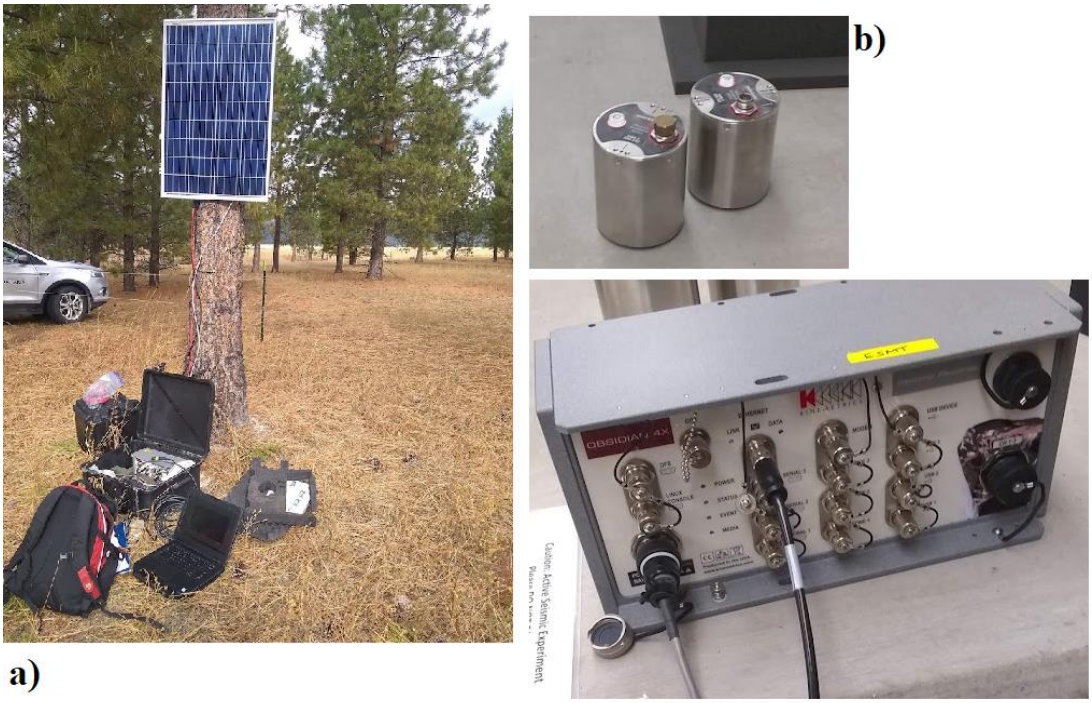

Figure S1. a) *Collection of seismic data in the field at a UMSN seismic station. Attached to the tree is the solar panel used to provide continuous power to the equipment. The black box at the base of the tree is where the digitizer is enclosed. In this photo, the field laptop is connected to the digitizer while downloading seismic data.* ***b)*** *Two Metrozet MBB-2 broadband, three-component, direct-burial seismometers from the UMSN that are deployed in the field.* ***c)*** *A Kinemetrics Obsidian 4X digitizer used to collect and store seismic data in the field.*

The data used in the inversion process are accessed from IRIS and analyzed with the Advanced National Seismic System (ANSS) Jiggle software, which provides a user interface that allows the user to analyze and download seismic data from multiple seismic networks. For both the west-central and regional models, we download seismic data collected by the UMSN, MRSN, USGS and ANSS for the time period July 2017 through May 2020. The initial format is written as an Hypoinverse .ARC file, which must then be converted to a .CNV file for input into the velocity model inversion software, VELEST. Appendix A shows an example of these files.

Earthquake phase arrival times from stations of the Transportable Array (TA) data were provided by Mike Stickney, Director of the Earthquake Studies Office at the Montana Bureau of Mines and Geology. Similar to the data retrieved from the ANSS Jiggle software, the TA phase data had to be converted to a readable Hypoinverse .ARC file and then converted to a .CNV file. An example of the original data and the formatted data is in Appendix A.

Supplementary Tables

Station	Latitude	Longitude	Elevation (km)	Station Correction (s)
BMMT	47.4907	-112.8763	1.676	0.00
BGMT	45.2333	-112.0400	2.172	-0.06
BRMT	47.1055	-113.2277	1.388	0.00
CLMT	46.8187	-112.6988	1.616	0.00
COMT	47.0788	-112.6144	1.665	0.00
EKMT	47.3505	-112.5383	1.473	0.00
ESMT	46.6567	-112.4426	1.742	0.00
FPMT	46.9988	-112.4026	1.660	0.00
GBMT	46.8592	-112.4568	2.235	-0.01
LGMT	46.8813	-112.6051	1.784	0.00
MVMT	47.0338	-112.9296	1.327	0.00
NVMT	46.7876	-112.5997	1.741	0.00
OGMT	46.8864	-112.8878	1.620	0.00
OVMT	47.0643	-112.9967	1.494	-0.07
CHMT	46.9143	-113.2520	2.077	0.07
LYMT	46.9700	-112.2895	2.237	0.02
BEMT	46.7483	-112.3300	2.228	-0.01
ALMT	47.0300	-114.4438	1.696	0.17
BHMT	47.5825	-115.0370	1.628	0.36
BLMT	48.0108	-114.3633	2.052	0.38
BPMT	46.4375	-113.4463	2.408	0.01

BSMT	47.8513	-114.7870	1.950	0.33
BZMT	45.6481	-110.7967	1.905	-0.12
CRMT	45.4558	-110.1402	2.941	-0.30
ELMT	46.5221	-112.4945	1.981	0.07
FBMT	47.4068	-114.4222	1.518	-0.01
HBMT	45.7930	-112.6078	2.481	0.54
HRY	46.7113	-111.8312	1.342	0.04
JTMT	47.7466	-114.2825	1.469	0.04
LCCM	45.8380	-111.8780	1.669	0.56
LDM	48.4538	-115.3191	0.840	-0.09
LRM	45.8221	-112.4510	2.326	0.49
MCMT	44.8276	-112.8488	2.323	0.23
MKMT	47.1031	-115.1138	2.088	-0.63
MOMT	44.5933	-112.3943	2.220	0.02
MSMT	45.6305	-110.3537	1.926	0.05
NDMT	47.2690	-114.7988	1.917	0.05
NQWL	44.8041	-111.5616	1.915	0.00
QLMT	44.8306	-111.4300	2.064	-0.01
SLMT	47.2418	-113.4935	1.701	-0.08
SWMT	47.5093	-113.9988	1.297	-0.31
SXM	46.1495	-111.2088	1.996	0.69
TPMT	44.7298	-111.6657	2.518	0.07
VCMT	46.4425	-114.1872	1.254	0.25
YBMT	47.8633	-114.0115	1.415	0.08
MSO	46.8292	-113.9406	1.264	0.20
MT01	46.9529	-112.6560	1.318	0.13
MT02	46.8585	-112.8804	1.672	-0.12
MT03	46.9129	-112.4970	2.025	-0.03
MT04	46.9554	-112.6560	1.402	0.00

Table S1. *Station corrections for all seismic stations used for the local velocity model.*

VELEST Inversion Parameters for the Local Velocity Model	
Parameter	**Value**

Number Of Iterations	6
Maximum Epicentral Distance	200 km
Minimum Hypocenter Depth	0.2 km
Maximum Adjustment of Layer Velocity	0.2 km/s
Maximum Adjustment of Hypocenter Depth	2.0 km

Table S2*: Inversion parameters used in the control file for the VELEST program. Epicentral distance refers to the distance from an event to a seismic station. The maximum adjustment parameters limit the amount of adjustment in depth or velocity allowed during each iteration. This selection of parameters yielded the lowest rms values for our preferred, final model.*

VELEST Inversion Parameters for the Regional Model

Parameter	**Value**
Number Of Iterations	9
Maximum Epicentral Distance	400 km
Minimum Hypocenter Depth	0.2 km
Maximum Adjustment of Layer Velocity	0.2 km/s
Maximum Adjustment of Hypocenter Depth	2.0 km

Table S3*. Inversion parameters used in the control file for the VELEST program for determining the regional-scale velocity structure for western Montana.*

Cluster	Num of Events	Dimensions	Trend	Distance from MS	Depth range	Date
1	2177	7.0 km by 9.0 km	N-S	0 km	10-20 km	7/17-5/19
2	67	0.5 km by 1.0 km	NNE-SSW	2 km (depth)	8-10 km	7/17-10/17
3	19	0.6 km by 0.4 km	NNE-SSW	7.8 km SE	12-15 km	7/17-10/17
4	5	0.1 km by 0.6 km	N-S	7 km N	15-18 km	5/18-6/18
5	6	0.2 km by 0.3 km	N-S	5 km W	7-8 km	10/18
6	5	0.3 km by 0.3 km	N-S	15 km NW	11-13 km	4/19
7	5	2.0 km by 2.0 km	NNE-SSW	7 km W	16-18 km	7/17-12/17
8	17	0.4 km by 0.9 km	N-S	12 km W	12-15 km	2/-19-4/19
9	12	1.5 km by 1.8 km	N-S	15 km W	15-17 km	7/17-10/17

10	10	0.5 km by 1.3 km	NNW-SSE	5 km SSE	19-21 km	1/17-8/17
11	6	0.2 km by 1.0 km	N-S	5 km E	12-15 km	11/17-5/18
12	4	0.2 km by 0.6 km	NNE-SSW	5 km E	16-17 km	11/18

Table S4*. Clusters, number of events, dimensions, cluster trend, distance from mainshock, depth range and time period for the double-difference relocations determined by Smith (2020).*

Appendices

Appendix A) Earthquake Phase Data Files

Example of earthquake data in .ARC format:

```
201707061959352346 5329112 3140 1303
DLMT IW  BHZ EP 4201707062000  247   5  0       0               0    1697 49         181        0    J  00
```

```
ALMT MB  EHZ EP 4201707061959 5958  32  0        0                  0    1466 69 0    52.1276207      0    JD 01
BEMT MB  EHZ IPU0201707061959 3969  -8158 4273ES 2 -44          19   0   0 214122          136       403  12J  01
BGMT MB  EHZ EP 3201707062000  525  47 13        0                  0    1877 49 0    49.5168211     16    JD 01
BHMT MB  EHZ EP 4201707062000  865 175  0        0                  0    2049 49 0    66.7293245      0    JD 01
BPMT MB  EHZ IPU0201707061959 4995 -10158        0                  0     864 97 0    49.8234189    381    JD 01
BSMT MB  EHZ EP 4201707062000  803 153  0        0                  0    2013 49 0    43.7303202      0    JD 01
CHMT MB  EHZ IPU0201707061959 4508   8158        0                  0     554101 0    64.7273208    301    JD 01
ELMT MB  EHZ IPD0201707061959 4275  12158 4825ES 2   8          19   0   0 408106 0    56.7176191    475  16JD
```

Relevant information:
First line represents the arrival time and information for the earthquake
20170706: year, month, day
19593523: hour, minute, seconds of origin time
46 5329: latitude
112 3140: longitude
1303: depth (meters)

Second line
DLMT: seismic station
IW: Network
BHZ: Component (vertical, North/South, East/West)
EP: P-wave (S for S-wave)
4: assigned p (or s) wave weight code
20170706: year, month, day
2000: hour, minute
247: second

Example of earthquake data in .PHA format:

```
# 2017  7  2  1 27 50.56  46.9072 -112.4540   12.58 0.90  0.65  0.90
0.14   0
MBBEMT      4.160  -1.000   P
MBBPMT     15.930   0.100   P
MBCHMT     10.730   1.000   P
MBELMT      7.960   0.200   P
```

Relevant information:
First line represents the arrival time and information for the earthquake
2017 7 2: year, month, day
1 27 50.56: hour, minute, seconds
46.9072 -112.4540: latitude, longitude
12.58: estimated depth
Second line represents the seismic station information:
MBBEMT: seismic network (MB), seismic station (BEMT)
4.160: seconds recorded after origin time
-1: weight of P (or S) wave arrival
P: P wave (S for S wave)

Example of MB network data that includes TA data in original MBMG format:

```
06 09 15  631  7.7 45.655 111.967 13.5 2.9 3.0     43  50  27.1 0.13  0.3  0.4 B MBMG
06091506
BEMTEP 3128.661
```

```
BGMTIPD3115.89         177.8
BPMTEP 3131.704
BSMTEP 3154.573
BUT EP-3118.112IS25.470
BZMTEP-3123.223
CHMTEPD3135.30         146.9
CRMTIPC3131.11         164.1
ELMTEPD3125.23         165.7
FBMTEP-3147.623
GCMTEP+3137.242
HBMTIPC3116.78         180.9
HRY EPD3127.29         182.2
```

Relevant information:
First line represents the arrival time and information for the earthquake
06 09 15: year, month, day
631 7.7: hour, minute, second
45.655 111.967: latitude, longitude
13.5: estimated depth
2.9 3.0: estimated magnitudes (coda duration and local)

Second line
06091506: year, month, day, hour

Third line
BEMT: seismic station
EP: P-wave
31: minute
28.661: second

Example of earthquake data in .CNV format (readable by VELEST):

```
17 7 6  630 16.78 46.8846N 112.5290W  17.65   5.80
DLMTP0 26.99BEMTP0  4.64BGMTP0 29.18BLMTP0 29.74BPMTP0 14.61BZMTP0
30.06 CHMTP0  9.85ELMTP0  7.54FBMTP0 24.94HBMTP0 20.65HRY P0  9.83JTMTP0
26.42 LCCMP0 21.66LRM P0 20.24LYMTP0  4.61MKMTP0 30.22NDMTP0 28.02NQBUP0
17.04 OVMTP0  7.33SLMTP0 14.15SWMTP0 21.29SXM P0 22.15VCMTP0 22.37YBMTP0
25.49 BOZ P0 25.44MSO P0 18.12
```

Relevant information:
First line represents information for the origin of the earthquake
17 7 6: year, month, day
630: hour, minute
16.78: seconds
46.8846N 112.5290W: latitude, longitude
17.65: estimated depth of hypocenter
5.80: magnitude of earthquake

Second line represents the arrival times recorded by the seismic stations
DLMT: name of individual seismic station
P0: the ‘P’ indicates it is a P-wave arrival and the ‘0’ represents the observation weight

26.99: seconds after the origin time when the station recorded the arrival of the wave
BEMT: indicates the next station. This pattern continues for the remainder of the example.

Appendix B) VELEST Files

Example of control file containing model parameters (parameters in bold have been set to recommended, default values):

```
******* CONTROL-FILE FOR PROGRAM V E L E S T  (28-SEPT1993) *******
***
*** ( all lines starting with  *  are ignored! )
*** ( where no filename is specified,
***   leave the line BLANK. Do NOT delete!)
***
*** next line contains a title (printed on output):
Lincoln, West-Central Model startmodell vers. 9.1
***      starting model 1.1 based on Castillo and Ellsworth 1993, JGR
***  olat       olon   icoordsystem      zshift   itrial ztrial    ised
46.8810     112.5749      0                1.830      0     0.00       0
***
*** neqs   nshot   rotate
      2500      0      0.0
***
*** isingle   iresolcalc
          0         0
***
*** dmax    itopo    zmin     veladj    zadj   lowveloclay
       200.0     0       -0.20       0.20    5.00         0
***
*** nsp    swtfac   vpvs       nmod
        1       0.50    1.760         1
***
***   othet   xythet    zthet    vthet   stathet
          0.01    0.01     0.01     01.0     0.01
***
*** nsinv   nshcor   nshfix     iuseelev    iusestacorr
         1          0         0            1             1
***
*** iturbo    icnvout   istaout   ismpout
           1          1           2        0
***
*** irayout   idrvout   ialeout   idspout   irflout   irfrout   iresout
           0          0          0          0          0         0         0
***
*** delmin   ittmax   invertratio
        0.010      06         1
```

Relevant parameter descriptions:
olat, olon: latitude and longitude of main event
zshift: used to shift hypocenters in depth relative to average station elevation (1830 meters, in this case)
neqs: number of earthquakes used in inversion
dmax: maximum epicentral distance
zmin: minimal depth for hypocenters to avoid 'air quakes'
veladj: maximum adjustment of layer velocity in each iteration step
zadj: maximum adjustment of hypocenter depth in each iteration step
lowveloclay: do not incorporate low-velocity layers
nsp: '1' tells the program to only use P-phases
vpvs: Vp/Vs ratio
ittmax: number of iterations

For greater detail on individual parameters, we refer the reader to the VELEST manual (Kissling *et al.,* 1994).

Example of seismic station file:

```
GBMT46.8592N 112.4568W    2235 1   2  -0.01   0.00
LGMT46.8813N 112.6050W    1784 1   3  0.00   0.00
NVMT46.7876N 112.5996W    1741 1   4  0.00   0.00
```

Relevant information:
GBMT: seismic station
46.8592N 112.4568W: coordinates of station
2235: elevation (meters)
2: station ID
0.24: station delay (p-wave)
0.00: station delay (s-wave, if applicable)

Example of input and output velocity models:

Input file:

```
Lincoln, West-Central Montana (mod1.1 EK280993)   Ref. station LGMT
8       vel,depth,vdamp,phase (f5.2,5x,f7.2,2x,f7.3,3x,a1)
4.80     -1.8   001.00          P-VELOCITY MODEL
5.37      1.0   001.00
6.05      5.0   001.00
6.16     10.0   001.00
6.33     15.0   001.00
6.58     20.0   001.00
6.77     25.0   001.00
7.00     30.0   001.00
```

Output file:

Output model:

```
        8
4.85     -1.80   1.000
5.37      1.00   1.000
6.03      5.00   1.000
6.17     10.00   1.000
6.33     15.00   1.000
6.58     20.00   1.000
6.77     25.00   1.000
7.01     30.00   1.000
```

8: represents the number of layers in the velocity model
The first column: seismic velocities in km/s
The second column: layer depths (a negative indicates above the surface)
Third column: damping factors (overdamping will fix the velocity layer in place)

Appendix C) HypoDD Files & Built-in Programs Used

ncsn2pha: Built-in program used to convert HypoInverse-2000 .ARC files (see Appendix A) to a .PHA file

ph2dt: Built-in program used to convert .PHA file to travel time differences used to determine event pairs recorded by a seismic station. Output of program used as input to HypoDD.

Input file for ph2dt:

```
* ph2dt.inp - input control file for program ph2dt
* Input station file: /home/es126387/hypoDD-files/MT-stations.txt
* Input phase file: lincoln-all.pha
*MINWGHT: min. pick weight allowed [0]
*MAXDIST: max. distance in km between event pair and stations [200]
*MAXSEP: max. hypocentral separation in km [10]
*MAXNGH: max. number of neighbors per event [10]
*MINLNK: min. number of links required to define a neighbor [8]
*MINOBS: min. number of links per pair saved [8]
*MAXOBS: max. number of links per pair saved [20]
*MINWGHT MAXDIST MAXSEP MAXNGH MINLNK MINOBS MAXOBS
        0.2          200          2            8            8            5            80
```

Control file for HypoDD containing adjustable parameters:

```
* RELOC.INP:
*--- input file selection
```

```
* cross correlation diff times:
*
*catalog P diff times: dt.ct
*
* event file: event.dat
*
* station file: MT-stations.txt
*
*--- output file selection
* original locations: all.loc
* relocations: all.reloc
* station information: all.sta
* residual information:
* all.res
* source parameter information:
* all.src
*
*--- data type selection:
* IDAT: 0 = synthetics; 1= cross corr; 2= catalog; 3= cross & cat
* IPHA: 1= P; 2= S; 3= P&S
* DIST:max dist [km] between cluster centroid and station
* IDAT IPHA DIST
    2         3      200
*
*--- event clustering:
* OBSCC: min # of obs/pair for crosstime data (0= no clustering)
* OBSCT: min # of obs/pair for network data (0= no clustering)
* OBSCC OBSCT
        0         8
*
*--- solution control:
* ISTART: 1 = from single source; 2 = from network sources
* ISOLV: 1 = SVD, 2=lsqr
* NSET: number of sets of iteration with specifications following
* ISTART ISOLV NSET
       2          1         2
*
*--- data weighting and re-weighting:
* NITER: last iteration to use the following weights
* WTCCP, WTCCS: weight cross P, S
* WTCTP, WTCTS: weight catalog P, S
* WRCC, WRCT: residual threshold in sec for cross, catalog data
* WDCC, WDCT: max dist [km] between cross, catalog linked pairs
* DAMP: damping (for lsqr only)
* --- CROSS DATA ----- ----CATALOG DATA ----
* NITER WTCCP WTCCS WRCC WDCC WTCTP WTCTS WRCT WDCT DAMP
```

```
     5        -9        -9        -9        -9        1.0       0.5       5         1         80
     5        -9        -9        -9        -9        1.0       0.5       5         1         80
*
*--- 1D model:
* NLAY: number of model layers
* RATIO: vp/vs ratio
* TOP: depths of top of layer (km)
* VEL: layer velocities (km/s)
* NLAY RATIO
     8        1.76
*UPT MODEL
* TOP
-1.80 1.0 5.0 10.0 15.0 20.0 25.0 30.0
* VEL
4.80 5.37 6.05 6.16 6.33 6.58 6.77 7.00
*
*--- event selection:
* CID: cluster to be relocated (0 = all)
* ID: cuspids of event to be relocated (8 per line)
* CID

* ID
```